AGU PUBLICATIONS

JGR

Journal of Geophysical Research: Atmospheres

RESEARCH ARTICLE
10.1002/2017JD027031

Key Points:
- A near-global satellite data set of marine low cloud is used to determine meteorological drivers of mesoscale cellular convection (MCC)
- A marine cold air outbreak index combining both surface forcing and lower tropospheric stability is shown to be a good predictor of MCC
- MCC types have different albedo-cloud fraction relationships indicating that mesoscale morphology is important for radiative impacts

Supporting Information:
- Supporting Information S1

Correspondence to:
I. L. McCoy,
imccoy@uw.edu

Citation:
McCoy, I. L., Wood, R., & Fletcher, J. K. (2017). Identifying meteorological controls on open and closed mesoscale cellular convection associated with marine cold air outbreaks. *Journal of Geophysical Research: Atmospheres, 122*, 11,678–11,702. https://doi.org/10.1002/2017JD027031

Received 26 APR 2017
Accepted 1 OCT 2017
Accepted article online 6 OCT 2017
Published online 3 NOV 2017

Identifying Meteorological Controls on Open and Closed Mesoscale Cellular Convection Associated with Marine Cold Air Outbreaks

Isabel L. McCoy[1], Robert Wood[1], and Jennifer K. Fletcher[2]

[1]Atmospheric Sciences, University of Washington, Seattle, WA, USA, [2]School of Earth, Atmosphere, and Environment, Monash University, Clayton, Victoria, Australia

Abstract Mesoscale cellular convective (MCC) clouds occur in large-scale patterns over the ocean and have important radiative effects on the climate system. An examination of time-varying meteorological conditions associated with satellite-observed open and closed MCC clouds is conducted to illustrate the influence of large-scale meteorological conditions. Marine cold air outbreaks (MCAO) influence the development of open MCC clouds and the transition from closed to open MCC clouds. MCC neural network classifications on Moderate Resolution Imaging Spectroradiometer (MODIS) data for 2008 are collocated with Clouds and the Earth's Radiant Energy System (CERES) data and ERA-Interim reanalysis to determine the radiative effects of MCC clouds and their thermodynamic environments. Closed MCC clouds are found to have much higher albedo on average than open MCC clouds for the same cloud fraction. Three meteorological control metrics are tested: sea-air temperature difference (ΔT), estimated inversion strength (EIS), and a MCAO index (M). These predictive metrics illustrate the importance of atmospheric surface forcing and static stability for open and closed MCC cloud formation. Predictive sigmoidal relations are found between M and MCC cloud frequency globally and regionally: negative for closed MCC cloud and positive for open MCC cloud. The open MCC cloud seasonal cycle is well correlated with M, while the seasonality of closed MCC clouds is well correlated with M in the midlatitudes and EIS in the tropics and subtropics. M is found to best distinguish open and closed MCC clouds on average over shorter time scales. The possibility of a MCC cloud feedback is discussed.

Plain Language Summary Low clouds are essential to the Earth system energy balance as they trap heat (outgoing energy) from the surface and reflect sunlight (incoming energy) to space. Global models incompletely capture low-cloud behavior, leading to large uncertainties in model predictions of future climate states. Improving predictions by reducing uncertainty is necessary for developing effective climate change adaptation/mitigation strategies. Our study investigates the environmental conditions influential to low-cloud development, relating easily modeled quantities to key development mechanisms for improving low-cloud model representations. Satellite-measured low clouds are grouped by their large-scale spatial structure using a pattern-recognizing program. The two primary cloud-type patterns are hexagonal with filled (closed) or empty (open) cells. Satellite and reanalysis data (models observationally constrained to real world) are used to examine their characteristics. Closed clouds reflect more sunlight than open clouds for equal cloud cover, indicating that energy balance contributions differ by cloud type and motivating the inclusion of low cloud by type in models. Energy from the surface and turbulence in the lower atmosphere influence open and closed cloud development. Large-scale motions of air from the high latitudes are particularly conducive to these clouds. M, an easily modeled parameter that quantifies this air motion, predicts open and closed cloud occurrences effectively and may be used to include low cloud by type in models and reduce prediction uncertainty.

1. Introduction

Marine boundary layer clouds are key influencers of the climate system. They have important radiative impacts through strongly enhancing shortwave reflection and trapping longwave radiation (Hartmann & Short, 1980). These radiative effects, as well as latent heat production through precipitation, play a key role in the global energy budget (Wood, 2012). Boundary layer clouds critically impact surface and top of atmosphere (TOA) energy budgets through their influence on the solar radiation budget in the high and midlatitudes, especially the Artic and Southern Ocean (SO) (Bennartz et al., 2013; Bodas-Salcedo et al., 2016).

The complex microphysics and dynamic processes of low clouds have garnered much interest in recent years because low clouds are a leading contribution to the uncertainty in the changing energy budget in climate models (Boucher et al., 2013). The model uncertainty from cloud feedbacks and cloud-aerosol interactions is due in part to difficulties in parameterizing the subgrid-scale processes important for these clouds (Boucher et al., 2013). Bias in modeling of surface and TOA radiative fluxes in the Southern Ocean (SO) is an excellent example of this problem and motivational for this work. Correct representation of the radiative fluxes in the SO is important for accurately predicting global warming effects in a coupled atmosphere-ocean model (Bodas-Salcedo et al., 2016; Trenberth & Fasullo, 2010). Problems in cloud amount and brightness in the SO result in radiation biases that lead to inaccurate energy budgets and atmosphere and ocean transport (Trenberth & Fasullo, 2010). SO biases are found to be associated with poor simulation of low and midlevel clouds, particularly those occurring in the cold sector of cyclones and in marine cold air outbreaks (Bodas-Salcedo et al., 2016, 2012; Field et al., 2011; Kay et al., 2016; Naud et al., 2014; Williams et al., 2013). Marine cold air outbreaks (MCAO) are movements of cold air from the poles equatorward over comparatively warmer water (Abel et al., 2017; Fletcher et al., 2016a). MCAO are known to influence development of low clouds as the warm water-cool air contrast increases the flux of energy and moisture from the surface into the boundary layer (Abel et al., 2017; Brummer, 1996; Fletcher et al., 2016b; Kolstad et al., 2009). Papritz et al. (2015) found that the seasonality and strength of the Southern Ocean turbulent heat flux (latent plus sensible heat flux) is strongly controlled by cold air outbreaks. Models are especially poor at simulating the supercooled liquid clouds that dominate the low-cloud population in the high latitudes, significant contributors to reflected shortwave radiation between 70° and 40°S (Bodas-Salcedo et al., 2016; Forbes & Ahlgrimm, 2014). Supercooled clouds are controlled by complex, subgrid-scale mixed-phase processes (e.g., nucleation, secondary ice formation, and Wegener-Bergeron-Findeisen) that are known to be poorly parameterized in models (Field et al., 2014; McCoy et al., 2016; Morrison et al., 2012). Some reduction in SO biases has been achieved by implementing improved microphysics and boundary layer schemes in certain models (Bodas-Salcedo et al., 2012; Field et al., 2014). This suggests that to find a complete solution to the SO and, more broadly, the midlatitude biases exhibited in models, a profound understanding of the processes associated with the clouds occurring in these regions must be developed. This understanding, especially of clouds in cyclone cold sectors and MCAO, could be used to further improve and implement parameterizations in models. As these clouds are in the "gray zone," where some model resolutions are growing close to the convective scale of the cells but may not resolve all the mesoscale circulations, parameterizations that comprehensively capture the multiple scales are important but difficult to achieve (Tomassini et al., 2016).

What clouds occur near and within these difficult to model, dynamic systems? To answer that, we first classify marine boundary layer clouds broadly based on their cellular morphology (Figure 1): open mesoscale cellular convection (MCC), closed MCC, no MCC, and cellular but disorganized cloud (Wood & Hartmann, 2006). Open and closed MCC clouds are organized into cellular patterns on the order of 10–40 km; cellular but disorganized has cellular clouds but lacks the large-scale organization of cells observed in open and closed MCC clouds; and no MCC clouds lacks both the cellularity and large-scale structure (Atkinson & Zhang, 1996; Wood & Hartmann, 2006). Open MCC clouds can be thought of as cumulus clouds arranged in hexagonal rings with a clear, descending region in the center. Closed MCC clouds are essentially hexagonally shaped cells of stratocumulus clouds arranged into a large-scale pattern with clear, descending cell edges (Atkinson & Zhang, 1996). Cellular but disorganized is the most prominent cloud type in this grouping, occurring over tropical regions in high quantities throughout the year. Crucially, open and closed MCC clouds dominate the midlatitudes and subtropical stratocumulus decks (e.g., Peruvian and Namibian) (Klein & Hartmann, 1993; Muhlbauer et al., 2014). These morphology types can loosely be thought of as different stages of the stratus to cumulus transitions observed over the eastern tropical and subtropical oceans (Wood, 2012). In the high latitudes and midlatitudes, a parallel transition is observed to occur between closed MCC clouds (stratocumulus-like) to open MCC clouds (cumulus-like). This transition is associated with the passage of cyclones and cold air outbreaks (Abel et al., 2017; Atkinson & Zhang, 1996; Field et al., 2014; Fletcher et al., 2016b). Closed and open MCC clouds dominate the midlatitudes and are potentially the difficult to model clouds associated with cyclones and cold air outbreaks (Fletcher et al., 2016b; Muhlbauer et al., 2014). Additionally, recent observations have confirmed that the stratocumulus/closed MCC cloud to open MCC cloud transition in cold air outbreaks often involves mixed-phase and supercooled clouds, adding complexity to parameterizing these clouds for the previously stated reasons (Abel et al., 2017).

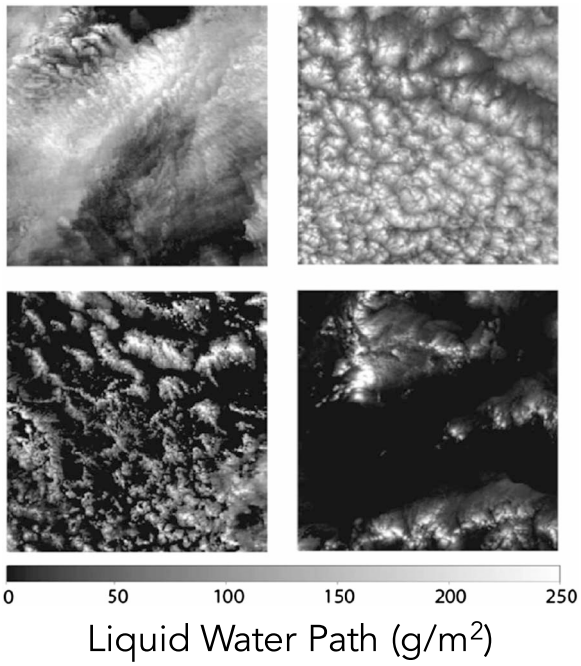

Figure 1. Example MODIS liquid water path subscenes identified by the neural network algorithm into (clockwise from top left): no MCC, closed MCC, cellular but disorganized, and open MCC clouds.

To improve understanding of how these clouds behave, one must understand the important drivers of open and closed MCC clouds. Mesoscale cellular convective clouds were first observed in the early 1960s with the dawn of the satellite era (Agee, 1984, 1987; Agee et al., 1973; Atkinson & Zhang, 1996). Open and closed MCC clouds have sufficiently large structures, with cell sizes often larger than 10 km, that satellites were needed to observe their distinctive patterns. Such cellular convection had only been observed in the laboratory prior to these satellite sightings (Atkinson & Zhang, 1996; Bénard, 1901; Graham, 1934; Rayleigh, 1916). Laboratory convective cells were first created by heating thin layers of fluid from below, producing thermal instability in the fluid, and letting surface tension (Bénard, 1901) and buoyancy (Rayleigh, 1916) effects create convection. Given this setup, it is not surprising that open and closed MCC clouds are an atmospheric parallel to the buoyancy-driven cellular convection, known as Bénard-Rayleigh cells, although real-world effects like latent heating create formation differences (Atkinson & Zhang, 1996). The complexities of these influences is aptly summarized by Agee (1987) at the end of his detailed comparison between laboratory and atmospheric cells:

> Similarities and differences have been duly noted, but atmospheric convection is subjected to a myriad of physical processes that are external to the thermally-driven convective overturning… Atmospheric convectionists should never fall into the trap of *categorically* stating that a particular convective structure is always caused by a single external forcing mechanism. Over and over this is seen not to be the case…

The important influences on MCC cloud development have become clearer since the 1960s and 1970s, particularly after the advent of large-eddy simulations (LES) and in situ observations. Many of the processes that are key in stratocumulus clouds are important for MCC clouds: shortwave heating and longwave cooling at cloud top; turbulence and entrainment; drizzle, latent heating and evaporative cooling; and surface fluxes of energy and moisture (Wood, 2012). Atmospheric static stability is also important and can be controlled by numerous factors including the cloud itself and synoptic meteorology. Open MCC clouds are particularly influenced by surface forcing, while closed MCC clouds are more affected by longwave cloud top cooling outside the subtropics (Kazil et al., 2014; Wood, 2012).

Two of the most investigated mechanisms for the transition and breakup of closed into open MCC clouds are (1) cloud-aerosol-precipitation interactions and (2) advection over warmer water (Yamaguchi & Feingold, 2015). These two mechanisms can be thought of as microphysically driven and large-scale meteorologically driven, respectively. The former has been substantiated through numerous LES modeling and observational studies (Berner et al., 2013; Feingold et al., 2010; Savic-Jovcic & Stevens, 2008; Stevens et al., 2005; Xue et al., 2008). Development of precipitation in closed MCC clouds can initiate cold pools, which spread out at the surface and interact. Collision of cold pools at the surface produces updrafts and an upward flux of energy and moisture. Closed MCC cloud begins to break up in locations of precipitation. In regions of enhanced surface forcing, cloud is sustained and forms the convective cells of new open MCC clouds (Berner et al., 2013; Savic-Jovcic & Stevens, 2008; Wood et al., 2011). Cold pools are not necessary for the closed to open transition to occur, as a recent LES study showed that precipitation applied evenly across the domain can also drive the transition (Vogel et al., 2016). This is consistent with precipitation being found a necessary but insufficient condition for this transition to occur (Wood, 2012; Yamaguchi & Feingold, 2015). Closed to open transitions may be influenced by aerosol suppression of precipitation in closed MCC clouds (Rosenfeld et al., 2006; Xue et al., 2008). Meteorological conditions, specifically stronger subsidence, can also suppress this transition by reducing the cloud thickness and preventing strong precipitation formation (Berner et al., 2013). The second, meteorologically driven mechanism involves the advection of cloud over warmer water (Bretherton & Wyant, 1997; Sandu & Stevens, 2011; Wyant et al., 1997). As the cloud moves over a comparatively warmer surface, an increase in the surface flux of moisture occurs. This liberates more latent heating in clouds,

driving stronger updrafts and enhancing cloud top entrainment of warm, dry free tropospheric air which drives boundary layer decoupling. Along with decoupling, liquid water path (LWP) is enhanced in geometrically thicker clouds which may additionally lead to precipitation (Bretherton & Wyant, 1997; Sandu & Stevens, 2011; Wood, 2012; Wyant et al., 1997). While these studies are of the subtropical stratocumulus to trade cumulus transition, a parallel can be made to the transition from closed to open MCC clouds (Yamaguchi & Feingold, 2015). This mechanism could explain the influence of large-scale meteorology in MCC cloud transitions seen in MCAO and cyclones (Atkinson & Zhang, 1996; Fletcher et al., 2016a; Muller & Chlond, 1996; Wood, 2012). Transitions from overcast stratocumulus to deeper, broken clouds have been observed in MCAO, consistent with the advection mechanism (Abel et al., 2017; Fletcher et al., 2016b). Examples of open and closed MCC clouds can be seen in the satellite imagery from the National Oceanic and Atmospheric Administration (NOAA) and National Aeronautical and Space Administration (NASA) GOES-16 satellite imagery in Figure 2. Classic transitions from closed to open MCC clouds are seen off California, South America, and in an MCAO from the Antarctic. The relative influence of precipitation and advection in these transitions is an open question as these mechanisms tend to occur together in varying degrees, making it difficult to distinguish the primary driver of open MCC cloud formation.

The objective of this paper is to develop a predictive metric for MCC clouds using our knowledge of meteorological and thermodynamic influences in the development of these clouds. It is important to note that prior work has found rather small differences in meteorology (i.e., lower tropospheric stability, vertical velocity at 850 hPa, and temperature advection) between open and closed MCC clouds in the subtropics (Wood & Hartmann, 2006). Meteorology is weaker in this region as well, suggesting the dominance of the precipitation mechanism and a potential zonal difference in the importance of these mechanisms. The lack of meteorological differences may also be explained if the differences driving transitions occur upstream of the transition of closed MCC clouds and development of open MCC clouds and disappear later. In this study, we examine the meteorology differences globally, especially focusing on the development of open and closed MCC clouds in the midlatitudes and high latitudes where MCAO and cyclones dominate. Although the precipitation mechanism is not investigated in detail, understanding where meteorology plays a dominant role will be enlightening for determining the regionality of these mechanisms and where each may be the primary influencer. Having a MCC cloud predictive metric may help to evaluate parametrizations of these clouds in weather and climate models, which both have considerable cloud-related biases (Fletcher et al., 2016a). As the impacts of these biases are radiative as well as structural (Bodas-Salcedo et al., 2012; Field et al., 2011; Williams et al., 2013), the radiative properties of MCC clouds were motivational for our work. The earlier work of Muhlbauer et al. (2014) on these properties is expanded upon. With a better understanding of the radiative characteristics of open and closed MCC clouds and their connection to MCAOs and cyclone cold sectors, we hope to make the sundry model biases more tractable.

In section 2, the data and methodology will be discussed. The MCC cloud identifications, reanalysis and satellite data, and the predictive metrics are all detailed here. Three meteorological control metrics are examined: estimated inversion strength, sea-air temperature difference, and an index for marine cold air outbreaks. Section 3 presents the results. In section 3.1 we introduce cloud fraction-albedo relationships for open and closed MCC clouds. Section 3.2 is a discussion of the MCC cloud seasonal cycle and what that suggests about the dynamical predictors of cloud morphology. Section 3.3 quantifies the relationships between MCC clouds and the predictor variables on synoptic scales. In section 3.4 we look at MCC cloud composites around cold air outbreaks and what this says about closed to open MCC cloud transitions. We conclude with a summary and discussion of our results and their implications in section 4.

2. Data and Methodology

2.1. Mesoscale Cellular Convection Identification

MCC cloud types are classified using the Wood and Hartmann (2006) neural network algorithm (NNA) applied to a full year of remotely sensed data in 2008. The essential elements of the NNA and analysis process are briefly described below; see Wood and Hartmann (2006) for complete details. This data set was also utilized in Muhlbauer et al. (2014). In both this work and Muhlbauer et al. (2014), the classification is assumed to be accurately identifying instances of MCC cloud at the same level as originally tested in Wood and Hartmann (2006) and with the same limitations. The NNA analyzes subscenes of retrievals from the National

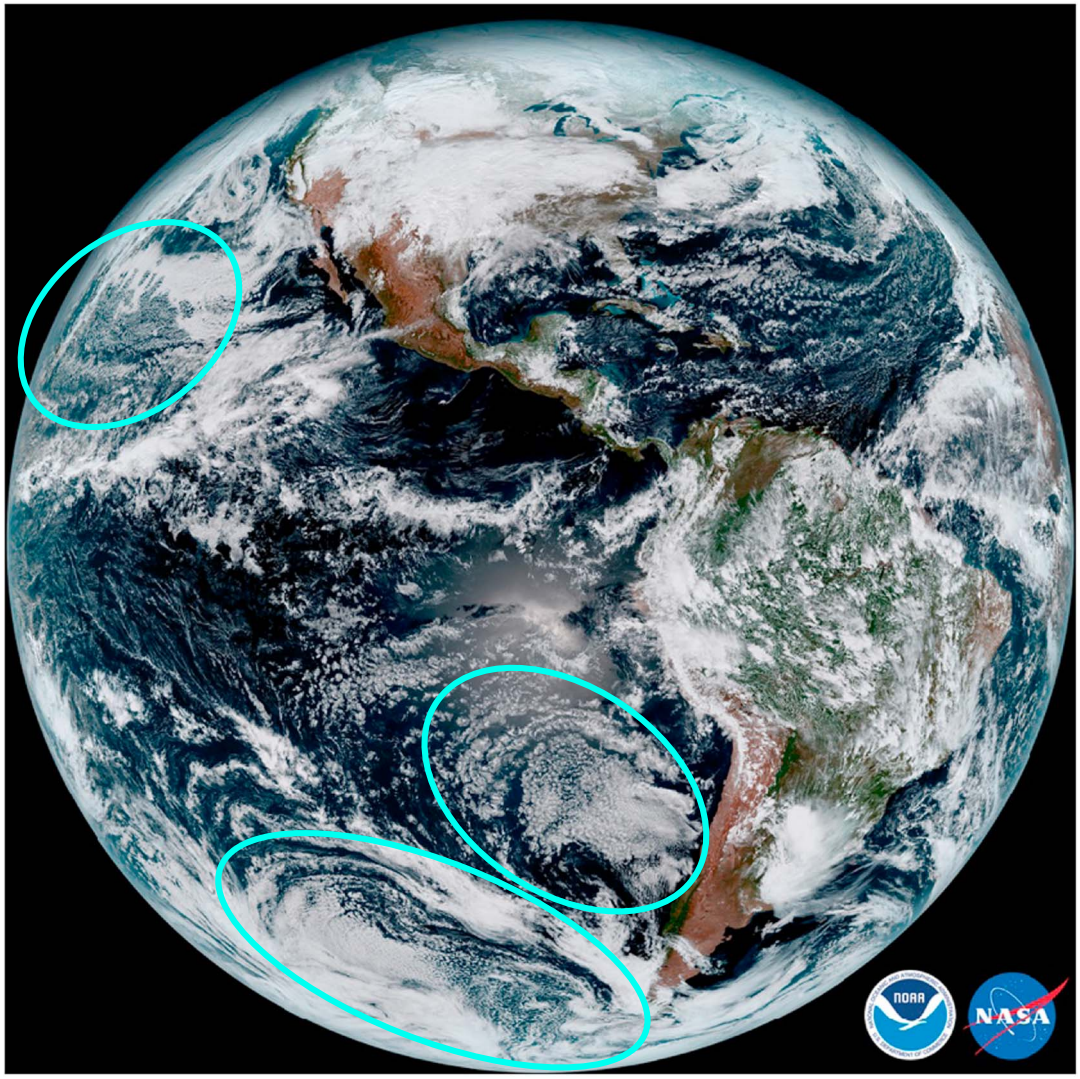

Figure 2. Visual imagery from NASA and NOAA's GOES 16 satellite (15 January 2017) (Leslie, 2017). Circles indicate occurrences of open and closed MCC clouds off (top) California, (middle) South America, and (bottom) in a cold air outbreak from Antarctica. Closed MCC clouds occur nearer to the coast and in the left quadrant of the outbreak before transitioning to open MCC clouds farther equatorward.

Aeronautic and Space Administration (NASA) Moderate Resolution Imaging Spectroradiometer (MODIS) Aqua satellite to determine cloud morphology (Platnick et al., 2003). Subscenes of the MODIS swath are 256 × 256 km^2 in size (oversampled by 128 km in each direction). Liquid water path (LWP) of each subscene, derived from cloud optical depth (τ) and effective radius (R_{eff}) retrievals, is used to classify low-cloud occurrences into the four morphology types discussed in section 1: open MCC, closed MCC, homogeneous or no MCC, and cellular but disorganized cloud (Figure 1). The probability density function (PDF) and power spectrum of the LWP in each subscene is calculated and used as inputs for the three-layer, back-propagating NNA. The use of both the PDF (a one-point statistic) and the power spectrum (a two-point statistic) of LWP is important for accurate cellular morphology identifications. The PDF describes the amount of liquid present and its homogeneity in the clouds. The power spectrum describes the spatial distribution of the LWP in the subscene, clearly marking the cellularity of MCC clouds and contributing a higher-order statistic to the analysis. Open MCC clouds have strongly skewed LWP PDFs and more high-frequency variance of LWP, making the PDF and power spectrum apt identifiers of this kind of MCC cloud (Wood & Hartmann, 2006). The NNA was previously trained and tested on 1000 human-identified cloud subscenes, split randomly into a testing and a training group. It has an 85–90% success rate in accurately

classifying subscenes into the four morphological types. Cases that are harder for the human observer to identify (i.e., those cloud subscenes that have features similar to more than one morphological type) account for many of the misidentifications (Wood & Hartmann, 2006).

In our study, the NNA is applied to the MODIS Aqua Collection 5.1 Level 2 cloud product for all marine data from 65°N to 65°S in 2008. The power spectrum analysis in the NNA requires the clouds to be contiguous. The NNA was trained on an earlier collection of MODIS where pixels on cloud edges were not systematically removed from the cloud product retrieval (King et al., 2003; Platnick et al., 2003; Wood & Hartmann, 2006). For consistency, the same method is applied for Collection 5.1. Missing cloudy pixels (i.e., those that have been determined *cloudy* or *probably cloudy* by the MODIS MOD35 mask but discounted by the MODIS MOD06 retrieved cloud fraction as insufficiently cloudy) are filled in the subscene through a LWP approximation that uses the retrieved LWP and the visual reflectance. A second-order polynomial fit of visible reflectance to the log of optical depth is developed from the retrieved pixels in the subscene. This fit is then used to compute optical depth for all the pixels in the subscene that have not been retrieved but are considered cloudy or probably cloudy according to the MOD35 cloud mask (Ackerman et al., 2002; King et al., 2003). Cloud droplet number concentration (N_d) is derived for the retrieved cloud pixels using the method of Bennartz (2007) and assuming adiabaticity of unity. The nonretrieved cloud pixels are assumed to have N_d equal to the median N_d of the retrieved pixels. Finally, the LWP of the missing cloudy pixels in the subscene is computed from N_d and τ using the equation (Grosvenor & Wood, 2014; Wood, 2006)

$$\mathrm{LWP} = \frac{1}{2}\left(\frac{\Gamma_{ad}\tau^6}{A^2k^2N_d^2}\right)^{1/5} \propto \left(\frac{\Gamma_{ad}\tau^6}{N_d^2}\right)^{1/5} \quad (1)$$

where $A \sim 0.0145$ and $k \sim 0.8$ are constants and $\Gamma_{ad} = \Gamma_{ad}(T,p)$ is the adiabatic rate of increase of liquid water content with respect to height. The LWP used in the NNA consists of the retrieved pixels and the broken and edge pixels that have been filled in through this method. As the optical depth from the logarithmic fit is necessarily nonzero, the application of a real-world lower bound to the derived LWP values is required before use. The MODIS instrument has an optical depth sensitivity of ~0.4 and an approximate maximum effective radius for low marine clouds of this nature of ~25 μm, which leads to an estimated detection limit of ~ 5 g/m^2 for LWP (Ackerman et al., 2008; Painemal & Zuidema, 2011; Wood, 2006). Instances of LWP $\leq$ 5 g/m^2 are assumed to be clear sky. The cloud fraction for each subscene is computed from the MOD35 cloud mask where the cloudy and probably cloudy flagged pixels of the scene are considered cloud (Ackerman et al., 2002). Pixels where LWP is below the above detection limit are considered clear sky in the cloud fraction (CF). MOD35 is used instead of the retrieved cloud fraction, MOD06, as it is a superior estimate for cloud fraction of broken clouds and more representative of the clouds identified by the NNA. The MODIS cloud mask uses both mean radiances and subpixel heterogeneity to determine the cloud mask markers, a more nuanced product than the MOD06 retrieved cloud fraction which is based on a reflectance threshold alone. In the original NNA in Wood and Hartmann (2006), only subscenes with cloud top temperatures above 273 K were considered usable, low-cloud cases (Ma et al., 2000). The restriction has been modified in this analysis to subscene cloud tops being within 30°C of the surface temperature, allowing classification of higher-latitude low clouds that have cooler cloud top temperatures and for the possibility of clouds with larger sea-air temperature differences. Subscenes are still restricted to having liquid cloud tops, however, which in combination with the cloud top temperature aims to ensure that no ice-topped cloud is analyzed. Many of the higher-latitude cloud with liquid tops are supercooled, and these may be mixed phase lower down in the cloud (Abel et al., 2017; Field et al., 2014). Thus, the microphysical characteristics of the higher-latitude clouds classified by the NNA could be substantially different from the more tropical clouds.

Quality screening was applied to the identification data before analysis. This included land and sea ice masking. The sea ice mask was generated based on monthly mean ice concentrations from the National Oceanic and Atmospheric Administration (NOAA) Optimum Interpolation (OI) Sea Surface Temperature (SST) V2 data set (Reynolds et al., 2002). Regions with monthly ice concentrations larger than 1% were masked out to obtain only the instances of cloud over water. In addition, regions where fewer than 50 data points (binned into 2.5 × 2.5° boxes) occurred over the year were excluded. The maximum number of points was ~500 in any given box. This ensured that enough classifications were made in any given area for the results to be representative of the region over the entire annual cycle. In total, there are ~800,000 subscenes globally and ~200,000 occurring between 60°S and 40°S.

There are several neural network algorithms to classify open and closed MCC cloud other than the one used in Wood and Hartmann (2006). Gufan et al. (2016) developed an alternative machine learning system and applied it to satellite observations of clouds previously identified as containing good cases of cellular morphology, an imagery analysis treatment of Geostationary Operational Environmental Satellite (GOES) data. Recent success has been achieved in morphology identification using PDFs of characteristic variables (Yamaguchi & Feingold, 2015). Their simpler methodology, which does not use the additional spectral analysis of Wood and Hartmann (2006), is designed to capture the closed to open cell transition and utilizes liquid water path, droplet number, and optical depth distribution modes and mode indexes as they evolve in time. While effective, this simpler methodology has only been demonstrated on idealized LES and not applied to observational data yet. The NNA from Wood and Hartmann (2006) remains the most applicable for the MODIS analysis presented here.

2.2. Reanalysis and Satellite Data

Reanalysis data are employed in this study to examine the large-scale meteorological and thermodynamic influences on cloud development. We used the European Center for Medium-Range Weather Forecasting (ECMWF) ERA-Interim data set (Dee et al., 2011). Four times daily data gridded to $1 \times 1°$ bins are used in the latitude range 65°N to 65°S for the full year of 2008. Reanalysis data are then collocated with the MCC cloud identifications by linearly interpolating the binned data to the individual identification points in space and time. The collocated reanalysis data, which are associated with the center of the subscene at the time of occurrence, is used to compute the meteorological controls (next section) associated with the NNA classifications. Note that ECMWF ERA-Interim data provides skin temperature instead of sea surface temperature, but they are equivalent over the ocean when no ice is present. This is referred to as sea surface temperature (SST) throughout this analysis.

Additionally, we utilized the Clouds and the Earth's Radiant Energy System (CERES) satellite data (Wielicki et al., 1996) to examine the radiative effect of the MCC clouds. Retrieved top of atmosphere shortwave flux and solar insolation from the Level 2 SSF Edition 4 Instantaneous footprints are used to calculate the instantaneous shortwave albedo (Wielicki et al., 1996). CERES follows closely behind MODIS Aqua in the A-train constellation, so the data is temporally well collocated. To spatially collocate the CERES and MODIS identification data, CERES pixels (~25 km circles) are sampled in a circle of 128 km radius centered on the middle of each of the square MCC cloud identification subscenes (256×256 km^2). This is similar to the method in Muhlbauer et al. (2014) for collocating data products of differing footprints. The albedo over the sampled circle is estimated as the average of the TOA SW flux for the footprints within the MODIS subscene divided by the average TOA solar insolation. This albedo includes the clear and cloudy sky associated with the MCC cloud classification. One disadvantage to using the circular average to calculate albedo for the identified subscene is that it misses the corners of the subscene and any cloud that may be occurring there. The albedo is associated more with the cloud in the center of the subscene, consistent with the NNA which primarily uses the subscene center when classifying due to the data windowing (Wood & Hartmann, 2006). However, this collocation methodology will add a systematic bias in comparisons between albedo and any other characteristics derived for the entire subscene (i.e., cloud fraction). The subscenes are relatively random samples of cloud fields; thus, one scene type (e.g., open MCC clouds) is not expected to have more cloud in the neglected corners than any other (e.g., closed MCC clouds). As a result, the bias will add variability to these comparisons but not change the mean.

2.3. Meteorological Control Metrics

Three meteorological control metrics are employed in our study, each capturing an aspect of large-scale dynamic and thermodynamic influences on MCC cloud development. They are estimated inversion strength (EIS), sea-air temperature difference (ΔT), and the marine cold air outbreak index (M) (Fletcher et al., 2016a; Kolstad & Bracegirdle, 2008; Wood & Bretherton, 2006). Each is calculated using reanalysis data. EIS is a measure of the strength of the boundary layer inversion, an indicator of the static stability of the lower atmosphere (Wood & Bretherton, 2006). It is a correction to the lower troposphere stability (LTS) metric, originally introduced in Klein and Hartmann (1993), which accounts for the tropospheric temperature profile. The tropospheric profile is assumed to have a structure closer to a moist adiabat rather than a dry one, resulting in a gradient that is more temperature sensitive. Wood and Bretherton (2006) found a strong linear relationship between EIS and cloud cover in the key stratocumulus regions across the globe. It has been recently

shown that EIS, along with being a good predictor of cloud cover in the relatively quiescent zones such as the tropics, is a good predictor of cloud cover in dynamically active regions behind cold fronts (Naud et al., 2016). EIS is calculated as in Wood and Bretherton (2006):

$$\mathrm{EIS} = \mathrm{LTS} - \Gamma_m^{850}(z_{700} - \mathrm{LCL}), \mathrm{LTS} = \theta_{700} - \theta_{1000} \quad (2)$$

In this equation, θ_{1000} is the potential temperature of the surface air, LCL is the lifting condensation level, and $\Gamma_{\mathrm{m}}{}^{850}$ is the moist adiabatic lapse rate at 850 hPa. Surface relative humidity, used in the LCL calculation, is approximated as 0.8 in light of its narrow distribution from 60°N to 60°S (Wood & Bretherton, 2006). The second metric, air-sea temperature difference (ΔT), indicates the contrast between the ocean and atmosphere heat content and is informative of the energy that could be fluxed from the ocean to atmosphere. This is simply the difference between the surface temperature and the 2 m temperature:

$$\Delta \mathrm{T} = T_{\mathrm{SST}} - T_{\mathrm{2m}} \quad (3)$$

The final metric tested is the MCAO index (M), originally defined by Kolstad and Bracegirdle (2008) and modified by Fletcher et al. (2016a) into temperature units. It is an index effective at identifying occurrences of marine cold air outbreaks. While somewhat similar to LTS (above), it is calculated at different pressure levels and uses the temperature of the sea surface instead of the air at the surface. This emphasizes the extreme temperature contrast between the cold polar air moving above comparatively warmer water, a dynamically favorable condition for planetary boundary layer cloud development. M is defined as

$$M = \theta_{\mathrm{SST}} - \theta_{800} \quad (4)$$

The effectiveness of these metrics as predictive factors for open and closed MCC clouds is tested in the subsequent section. An example of M, EIS, and ΔT values and the associated MCC cloud identifications in a Southern Hemisphere winter marine cold air outbreak is shown in Figure 3. The cloud field shown in this example is midway through a transition from closed to open MCC cloud under the influence of the MCAO, a plume of cold air moving counterclockwise from the higher latitudes (35°S) to the lower latitudes (20°S). Assuming that the wind is in near-geostrophic balance, the flow approximately follows the sea level pressure (SLP) contours (arrows in Figure 3d). As the cold air moves from high to low latitudes, it passes over increasingly warmer SSTs (Figure 3d). The MCAO both disrupts the stability of the boundary layer and moves the closed MCC clouds over the warming ocean in its path. The latter can be seen by the cloud field filling out the outbreak plume, which matches the shape of the SST and SLP patterns in Figure 3d. We expect, from the theories presented earlier, that a decreasing stability caused by the motion in the MCAO and increasing surface forcing due to the warmer ocean-cooler air temperature contrast will encourage the closed MCC clouds to transition to open MCC clouds. In this example, locations where the atmosphere has been affected by the meteorology for longer (bottom right) or is strongly forced by the SSTs (top left) have already transitioned. Of the metrics, M (Figure 3a) best coincides with the expected MCC occurrences and the cold air outbreak expanse (as inferred from the SST and SLP pattern in Figure 3d). The strongest M values, weakest stability (EIS, Figure 3c), and largest surface forcing (ΔT, Figure 3b) occur in the most sustained region of the outbreak (bottom right) and are associated with the most open MCC clouds in the scene. The weakest M values, larger EIS, and weaker ΔT occur at the edge of the cold air outbreak (middle and left) and are associated with more closed MCC clouds. The alignment of MCC clouds and the behavior of the variables in this example are in keeping with the theory of meteorological influence on MCC clouds discussed in section 1, and the importance of surface forcing for the development of open MCC clouds is particularly demonstrated.

3. Results

3.1. Cloud Fraction-Albedo Relations

Many studies have demonstrated that fractional cloud cover is a useful quantifier of cloud radiative effect. Hartmann and Short (1980) originally showed the relation between cloud fraction (CF) and total or all-sky albedo and the subsequent cloud impact on radiative balance. More recently, variations in CERES all-sky albedo and MODIS cloud fraction were found to be well correlated (Loeb et al., 2007). This suggests that globally, cloud cover anomalies are a good proxy for all-sky albedo. From these and other works, we would expect the radiative effect of open and closed MCC cloud to be primarily determined by their CF. Open and closed MCC clouds have overlapping distributions of cloud cover with closed MCC clouds having larger mean CF

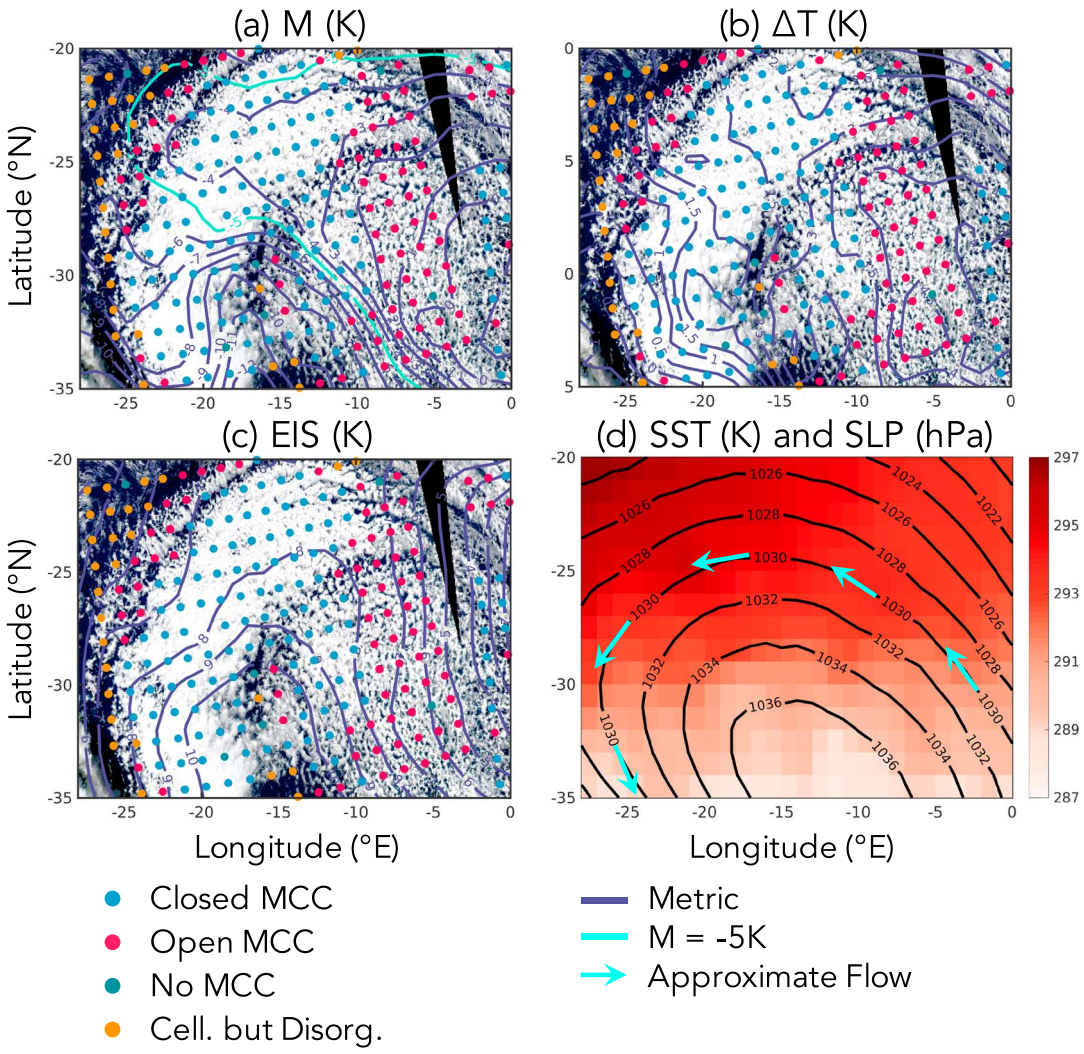

Figure 3. Example marine cold air outbreak occurring in the Southern Hemisphere winter (13 August 2008). MCC cloud identifications are overlaid on MODIS Aqua surface reflectance with contours of meteorological control metrics (in K): (a) ΔT, (b) EIS, and (c) M. Identifications are colored by type: closed MCC (blue), open MCC (red), no MCC (green), and cellular but disorganized (yellow) clouds. The $M = -5$ K contour marks the edge of the strongest part of the cold air outbreak. (d) Surface temperature and sea level pressure contours show the approximate flow (arrows following SLP assuming geostrophic balance) of cold air over warming water.

than open MCC clouds (Figure 4, bottom) (Muhlbauer et al., 2014). Where open and closed MCC clouds occur with the same CF, we would expect a similar scene albedo based on the above logic. Similar cloud fractions in open and closed MCC clouds are very likely to occur across the globe (Figure 4, bottom). One reason is that the size of individual cloud cells comprising the large-scale MCC cloud pattern can change with boundary layer depth (Muhlbauer et al., 2014; Wood & Hartmann, 2006). A spreading of the MCC pattern will occur for deeper boundary layers, modifying the cloud fraction and producing a spread in possible CF for a given type.

Such a qualitative analysis does not consider macrophysics (e.g., liquid water path, LWP) or microphysics (e.g., droplet concentration, N_d) known to be contributing factors to the cloud albedo (Boers & Mitchell, 1994; George & Wood, 2010; Wood, 2006). Indeed, when examined in PDF form, the microphysical and radiative characteristics of open and closed MCC clouds suggest large differences between types. For example, closed MCC cloud has more frequent light drizzle, while open MCC cloud has a higher fraction of heavy drizzle. Closed MCC cloud also tends toward higher shortwave reflectance than open MCC cloud, but the magnitude of reflectance and difference between NNA-determined cloud types changes regionally (Muhlbauer et al., 2014). A technique for quantifying cloud radiative effect while considering the contribution of microphysical

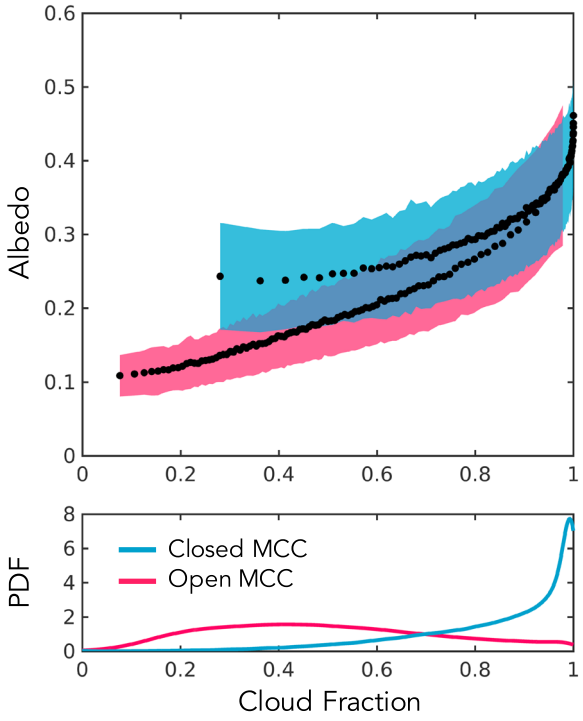

Figure 4. (top) Quantiles of cloud fraction versus subscene albedo for open (red) and closed (blue) MCC clouds globally (65°S to 65°N) for 2008. Black dots indicate mean albedo within CF quantile bins; variability of data is shown with 1σ shading. (bottom) Probability distribution function of CF for open and closed MCC clouds in the same region and time.

and macrophysical variations of the cloud is to develop an explicit relationship between the cloud fraction and the all-sky albedo (Bender et al., 2011, 2017, 2016; Engstrom et al., 2015, 2014; Webb et al., 2001). The observed spread in total albedo for any fixed cloud fraction will be due primarily to the variability in factors affecting the optical depth of the cloud (Bender et al., 2016). Solar zenith angle will affect the albedo as well, particularly in high-latitude, high cloud fraction cases (Bender et al., 2017; Engstrom et al., 2015). A correction can be made to remove this influence from the variability but should be kept in mind otherwise (Bender et al., 2017). A simple separation into cloud types was accomplished in prior analysis by choosing stratocumulus-dominant regions to investigate (Bender et al., 2011, 2016; Engstrom et al., 2014). However, these relationships have not been separated based on MCC cloud type or cloud morphology explicitly. In future work, we can use these relations to address whether the higher shortwave reflectance of closed MCC clouds is due more to cloud fraction or microphysical and macrophysical reasons.

It is immediately apparent that the CF-albedo relationships are different for open and closed MCC clouds (Figure 4). For a given cloud fraction closed MCC cloud tends to have a higher scene albedo than open MCC cloud, confirming our suspicion that the scene albedo of different MCC cloud types is not determined by cloud fraction alone. Each cloud type can assume a wide range of cloud fractions. The distribution of scene albedo around the means partially overlaps between cloud types at higher cloud fractions. It is likely that the few open MCC clouds identified at these very high CF have been captured immediately post transition from closed MCC clouds. These cases, relating back to the original discussion of the NNA and its limitations, would be part of the "harder to identify by eye" portion of the scenes. However, for cloud fractions between 0.5 and 0.8, both cloud morphologies occur frequently (26% of closed MCC clouds and 34% of open MCC clouds, see probability distribution function of CF in Figure 4) and are well separated in scene albedo (by 0.05 on average). What is the potential effect of the albedo difference between open and closed MCC clouds? Assuming typical incoming solar radiation is ~340 W m^{-2}, this 0.05 difference in scene albedo between types would lead to ~17 W m^{-2} reflected to space dependent on MCC cloud type for the same cloud fraction. Estimating the Southern Ocean shortwave cloud radiative effect as ~ −70 W m^{-2} (Hartmann, 2016), this is a significant change (~24% change in radiative effect from switching between open and closed MCC clouds excluding the change in CF that could occur).

How do the MCC cloud CF-albedo curves compare to the CF-albedo relationships found for all low clouds (Bender et al., 2011, 2017, 2016; Engstrom et al., 2015, 2014; Webb et al., 2001)? Even though the low-cloud relationships are for different time averages (annual and monthly means) than the MCC cloud curves, it is still instructive to compare. Marine low clouds are found to have a quasi-exponential relationship between CF and all-sky albedo globally when averaged over a long period (2002–2014) (Engstrom et al., 2015). While MCC cloud CF-albedo curves have exponential traits as well, the curve shape changes significantly between type and would not be well described by one exponential. Clearly, grouping all low-cloud types together results in morphological differences being obscured. This suggests that using a low-cloud CF-albedo relationship to evaluate models may have limitations in the eventuality of improved low-cloud parameterizations being implemented (particularly if MCC clouds are parametrized). Zonal differences exist in the global low-cloud relationships: midlatitudes contribute to the top of the curve (high CF and high albedo), subtropics to the middle, and tropics to the bottom (lower cloud fraction, lower albedo) (Bender et al., 2017). MCC cloud CF-albedo relationships are broadly consistent, exhibiting similar zonal differences to Bender et al. (2017) (not shown). The near-exponential CF-albedo relationship for low clouds indicates that albedo sensitivity to increases in cloud cover increases strongly with cloud fraction (Bender et al., 2017; Engstrom et al., 2015), as seen in other studies (Webb et al., 2001). As the MCC cloud CF-albedo relationships are quasi-exponential, they will have a similar sensitivity. The sensitivity of open and closed MCC clouds may be different, however, as they are not described by the same curve and have different rates of increase with CF. There are several

interesting possibilities for why there are large differences in albedo between cloud morphologies even for the same CF, but these will be investigated in more detail in subsequent work.

3.2. MCC Climatology

The first step to understanding MCC cloud is to observe the location and frequency of their occurrence. Klein and Hartmann (1993) established the spatial distribution of low-cloud cover and its seasonality but did not distinguish between types of low cloud. Muhlbauer et al. (2014) focused on the seasonal frequencies of open, closed, and cellular but disorganized MCC clouds. We expand that work by identifying the magnitude and phase of the seasonal cycle globally for open and closed MCC clouds. Consistent with Muhlbauer et al. (2014), a cloud occurrence frequency is defined as the number of times a cloud type (e.g., open MCC cloud) is observed in a region and time period (e.g., over a month) divided by the number of times all NNA-identified cloud types occur in that region and time:

$$f_{\text{type}} = n_{\text{type}} / \left(n_{\text{open}} + n_{\text{closed}} + n_{\text{noMCC}} + n_{\text{disorganized}} \right) \tag{5}$$

Monthly frequencies were calculated in every $5 \times 5°$ grid box for open and closed MCC clouds. This grid box size is chosen to properly allow for the 2.5° scene identifications. The annual average of f_{open} (open MCC cloud occurrence frequency) and f_{closed} (closed MCC cloud occurrence frequency) can be seen in Figures 5a and 5b, respectively. Closed MCC clouds are most predominant in the persistent stratocumulus regions marked by the Klein-Hartmann boxes (Klein & Hartmann, 1993), as previously observed by Muhlbauer et al. (2014) and Atkinson and Zhang (1996). This is consistent with the idea that closed MCC clouds most commonly occur over cold water to the west of continents, regions of strong stratocumulus decks (Atkinson & Zhang, 1996). Open MCC cloud is more uniformly distributed across the globe. A shift from f_{closed} to f_{open} is seen further west and equatorward of the closed MCC cloud regions, the areas of stratocumulus breakup (Bretherton & Wyant, 1997; Wyant et al., 1997; Yamaguchi & Feingold, 2015). Cellular but disorganized cloud is the most frequent type identified, occurring prominently in the tropics (Muhlbauer et al., 2014). Clouds without MCC are infrequently observed, the rarest of the four classification types. These last two NNA classification cases do not contain the organized cellular morphology of interest and so will not be discussed further in this analysis. Because of their ubiquity, especially in the midlatitudes, understanding the forces and controlling meteorology driving open and closed MCC cloud occurrences is important.

We examine the seasonal cycle to help determine the meteorological factors in MCC cloud development. A sinusoidal least squares curve fit with a fixed 1 year periodicity was applied to the monthly mean MCC cloud frequencies in each grid box. From this fit we determined the amplitude (half the difference between maximum and minimum) and peak month of cloud occurrence for both types. The seasonal cycle amplitude and associated season of peak occurrence is shown for f_{open} (Figures 5c and 5e) and f_{closed} (Figures 5d and 5f). The pattern of seasonality and peak season is consistent in the midlatitudes and becomes more variable and statistically insignificant in the subtropics and tropics for both closed and open MCC clouds. f_{open} has the largest seasonal cycle in the midlatitudes consistent with the observations in Muhlbauer et al. (2014). Open MCC clouds exhibit a monthly maximum in occurrence in the hemisphere winter (December-January-February (DJF) in the Northern Hemisphere (NH) and June-July-August in the Southern Hemisphere (SH)). The seasonality and peak season are more varied and less significant in the tropics for open MCC clouds. f_{closed} has the largest seasonal amplitude in the Klein-Hartmann boxes and upper midlatitudes. In the midlatitudes, they peak in the summer of the appropriate hemisphere (June-July-August for the NH, and DJF for the SH). Similar to f_{open}, the f_{closed} seasonal cycle and peak time of occurrence are not coherent and statistically significant in the subtropics and tropics. The southeast Pacific (SEP) and southeast Atlantic (SEA) are the two regions of exception, with somewhat coherent patterns of seasonality peaking in September-October-November. The ill-defined seasonal pattern of both MCC cloud types in the tropics is not entirely unexpected as the meteorology and dynamics in that area predominantly favor cellular but disorganized clouds (Muhlbauer et al., 2014).

The timing and location of the open MCC cloud seasonality is consistent with a strong connection to marine cold air outbreaks. MCAOs occur in the high latitudes and midlatitudes, with cold air plumes traveling up even into the subtropics. They also peak in hemisphere winters. The spatial and temporal parallels between open MCC clouds and MCAOs is in line with earlier theories in the literature (Agee, 1987; Atkinson & Zhang, 1996; Muhlbauer et al., 2014; Wood, 2012). We will quantify this relationship in the following section.

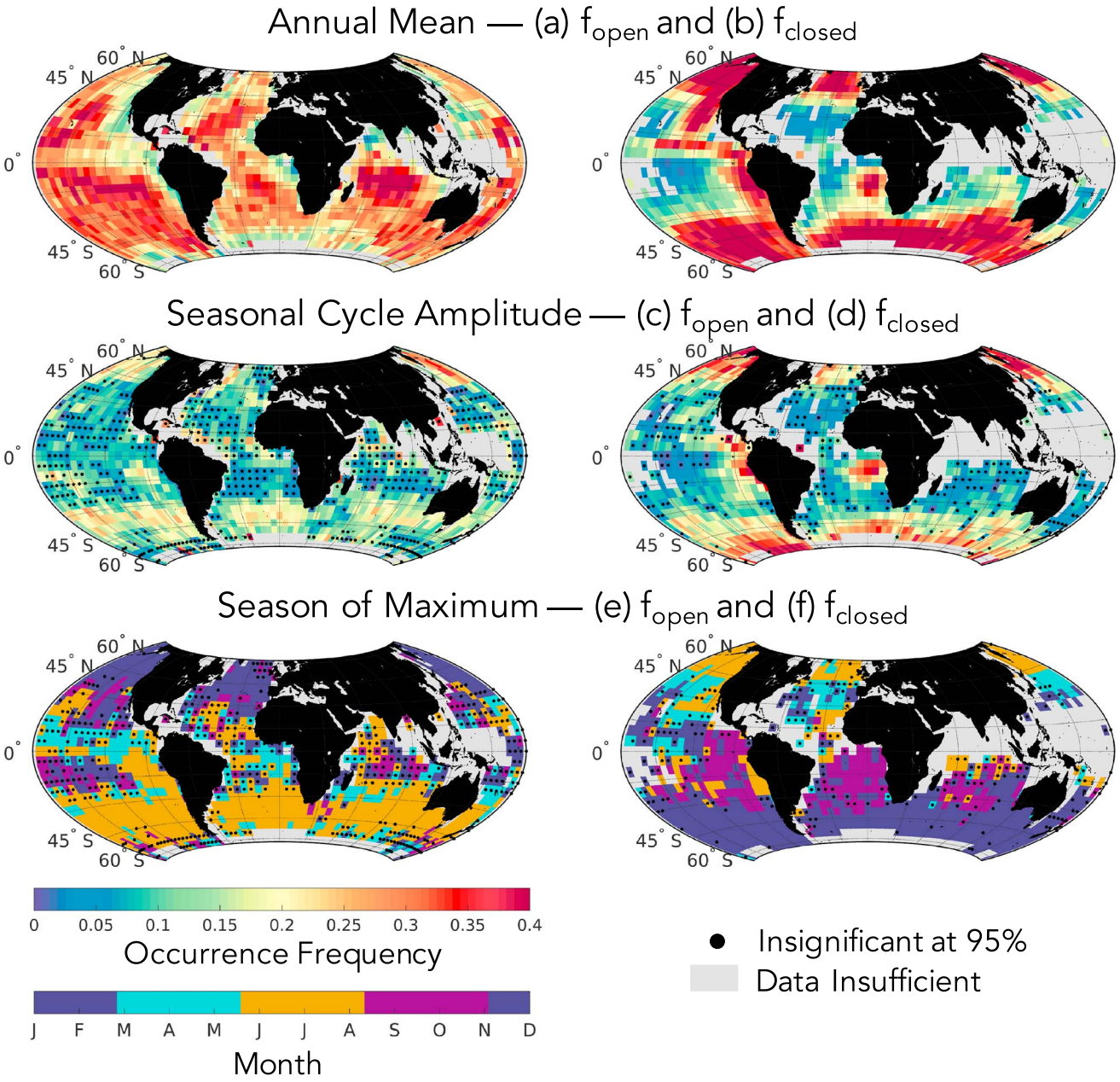

Figure 5. (a, c, and e) Open and (b, d, and f) closed MCC cloud climatologies: annual mean frequency (Figures 5a and 5b), seasonal cycle amplitude (Figures 5c and 5d), and season of peak frequency (Figures 5e and 5f). Gray areas indicate where there is insufficient data retrieved and classified in 2008 to make an accurate estimate of the frequency. Black dots are where the fit and subsequent results are not significant at a 95% confidence level. Confidence is determined based on a Poisson count method using the number of occurrences.

3.3. MCC Relationship to *M*, EIS, and ΔT

In this section, we compare the seasonal cycles of different cloud morphologies with the seasonal cycles of our three meteorological control variables: EIS, ΔT, and M. Correlation coefficients between the sinusoidal seasonal fit of the MCC cloud frequency (shown in Figures 5c and 5d) and the three metrics indicate where the strongest seasonal cycle relationships exist across the globe (Figure 6). For all metrics, especially ΔT and M, the largest coherent pattern of seasonal cycle correlations with MCC clouds occurs in the midlatitudes. The exception to this is the f_{closed}-EIS correlation in the SEP and SEA (Figure 6d). This strong pattern suggests that closed MCC clouds in these regions are more sensitive to static stability than surface forcing, consistent with the strong CF-EIS relationship found in these regions (Wood & Bretherton, 2006). This is consistent with the

tendency for closed MCC clouds to have slightly larger stability than open MCC clouds but little difference in temperature advection or other characteristics of large-scale meteorology in these regions (Wood & Hartmann, 2006). The f_{open}-M correlation (Figure 6e) is particularly large and significant over the midlatitudes, consistent with the theory connecting them to cold air outbreaks which occur frequently and have strong seasonality in this region (Fletcher et al., 2016a).

The midlatitudes are the largest region of correlation for the seasonal cycles and thus warrant a more extensive examination (Figure 7). The mean and variability of monthly f_{closed}, f_{open}, EIS, ΔT, and M averaged across the NH (30°–60°N) and SH (30°–60°S) midlatitude bands are shown in Figure 7 (a and b for occurrence frequencies; c–e for metrics). The seasonality of the NH has been shifted back by 6 months to align with the SH seasonality. Variability is a combination of spatial, from the latitude bands, and submonthly. For example, differences between monthly standard deviations in the NH will be associated with the temporal variability while differences between NH and SH standard deviation for the same month are associated more with spatial variability. The seasonal cycle correlation coefficients for the combined midlatitudes and separate NH and SH midlatitudes are located in Table 1 and are significant at 95% confidence level for a 24- and 12-point correlation, respectively. Examining the combined midlatitude correlations first, both f_{open} and f_{closed} have the strongest seasonal cycle correlation in the midlatitudes with M. ΔT ranks a close second everywhere except the SH where EIS is comparable (f_{open}) or superior (f_{closed}) to the other metrics. The effectiveness of EIS in the SH is largely connected with the edges of the SEA and SEP regions, already noted to be regions dominated more by stability than surface forcing. EIS is especially weak in the NH, weakening the combined correlation for both f_{open} and f_{closed}. The results in Figure 6 elucidate these relationships. Surface forcing (ΔT and M) appears much more important for f_{closed} in the NH than stability (+EIS), which leads to the weakened overall correlation for EIS (Table 1). The larger surface forcing is likely due to the stronger land-sea contrast in the NH enhancing cold air outbreaks, especially in the NEA as seen in Figure 6b. This enhancement can also be seen in the larger amplitude of the ΔT seasonal cycle in the NH compared to the SH (Figure 7e). Surface forcing and instability (-EIS) are clearly both important for these cloud types, making the combined effect, captured by M, superior. This is especially true for f_{open} whose correlations with M are a larger improvement from a simple stability relationship than for f_{closed}. Overall, the variability of the metrics is much larger in the winter for M, ΔT, and f_{open} and in the summer for EIS and f_{closed}. All metrics have larger seasonal amplitudes and variability in the NH than the SH, particularly ΔT. The frequencies are more consistent across hemispheres than the metrics, although f_{closed} has slightly more variability in the summer NH compared to SH. Note that a similar analysis was performed on the tropics, but the incoherent seasonal cycle correlations that exist across 30°S to 30°N (see Figure 6) are not found to be significant when the tropical band is considered as a whole. The consistently robust positive seasonal correlation between M and f_{open} globally suggests that M is a good open MCC cloud seasonality predictor. M may also be a good predictor for closed MCC globally, but it is best in the midlatitudes. EIS also has merit for prediction of subtropical closed MCC cloud seasonality.

As an aside, a notable reduction in f_{open} and increase in f_{closed} occurs in the midwinter in the Northern Hemisphere (occurring on the left side of W in Figure 7 panels, recalling that the NH time is shifted back 6 months). This reduction may be the result of a midwinter lull in storm activity that can occur in the Pacific basin in the NH at this time (Nakamura, 1992). The tropospheric jet maximizes in winter over the Pacific. When the jet grows too strong, suppression of baroclinic waves will occur and reduce the meridional flux of heat and zonal momentum (Nakamura, 1992). The midwinter suppression negatively affects the storminess in the Pacific storm tracks (i.e., midlatitude cyclones and associated cold air outbreaks) (Nakamura, 1992; Penny et al., 2010). A plateauing of M and increase in EIS consistent with this theory is clearly observed during the same midwinter period as the f_{open} decrease and f_{closed} increase (Figures 7c and 7d). The MCC cloud frequency behavior may be evidence for the influence of midwinter baroclinic wave suppression on low-cloud fields.

To explain why M has a strong seasonal cycle correlation with both open and closed MCC clouds in the midlatitudes, we can examine the relations between M, EIS, and ΔT. Recall that M is an estimate of the strength of a cold air outbreak, EIS estimates the static stability, and ΔT estimates the strength of surface heating. M can be written with a few approximations as a function of EIS and ΔT using equations (2)–(4):

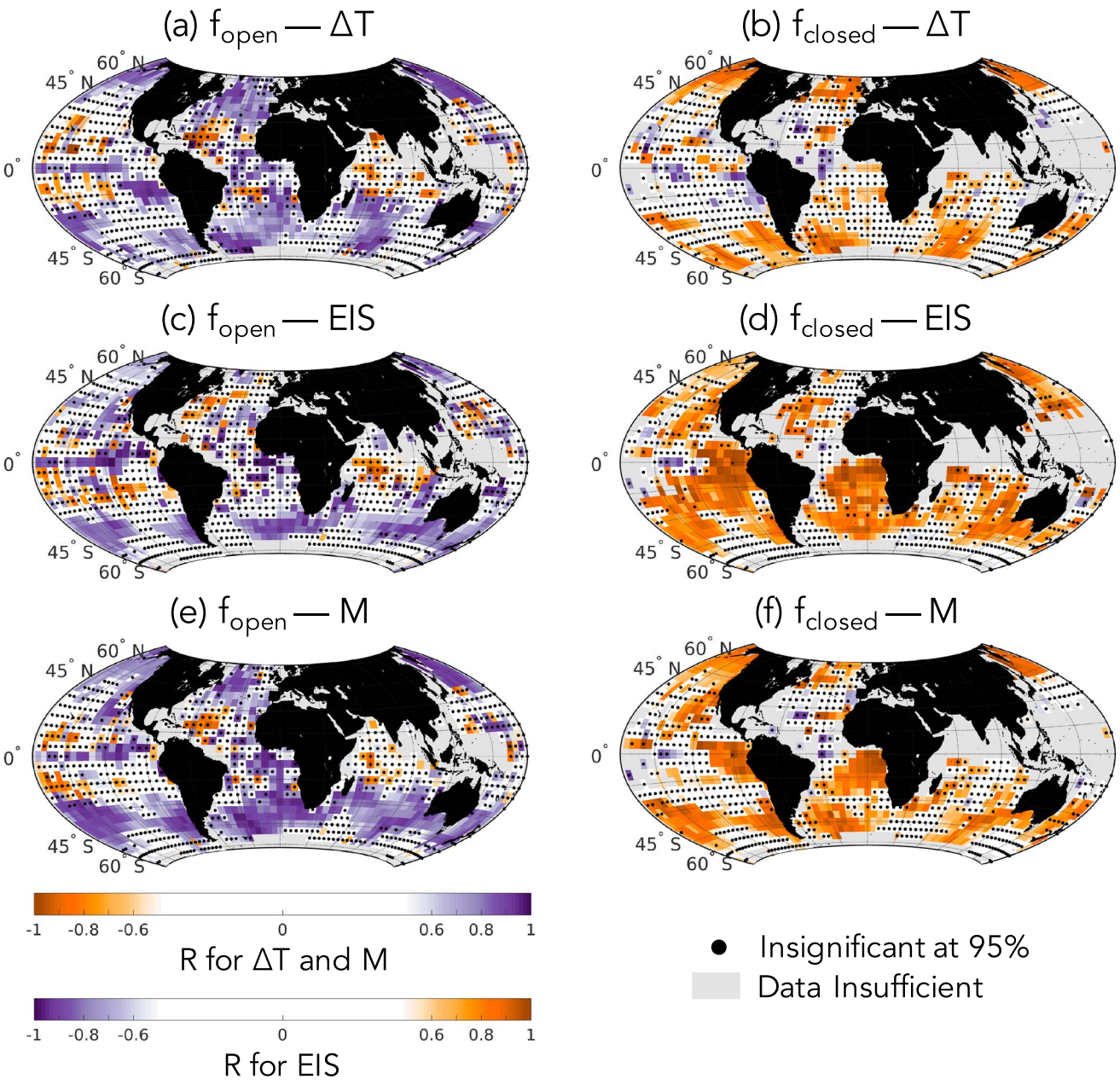

Figure 6. Seasonal cycle correlation coefficients between (a, c, and e) open and (b, d, and f) closed MCC cloud occurrence frequency fits from Figure 5 and meteorological control metrics: ΔT (Figures 6a and 6b), EIS (Figures 6c and 6d), and M (Figures 6e and 6f). As in Figure 5, gray indicates where insufficient data and dots where fit is insignificant. White is where the correlation is not significant for 12 points (all months).

$$M = \left(\frac{1000}{p_0}\right)^{R/c_p} \Delta T - EIS - \Gamma_m^{850}(z_{800} - LCL) \sim \Delta T - EIS + const. \quad (6)$$

The relationship between these three metrics for each cloud type is graphically shown with two-dimensional histograms of M by ΔT and EIS (Figures 8a and 8b). Each histogram is calculated using a composite of the MCC cloud identified data for the global, yearlong data set. All subscenes, from the midlatitudes, subtropics, and tropics are included (65°S to 65°N). The M-ΔT-EIS relationship is shown separately for open and closed MCC clouds but are nearly identical as equation (6) shows (Figures 8a and 8b, respectively). In both cases, M depends equally on EIS and ΔT in corroboration with the linear equation derived for M (equation (6)). We can also examine the dependence of open and closed MCC cloud occurrence frequency on EIS and ΔT (Figures 8c and 8d, respectively). f_{open} (Figure 8c) mimics the shading of the associated M in Figure 8a,

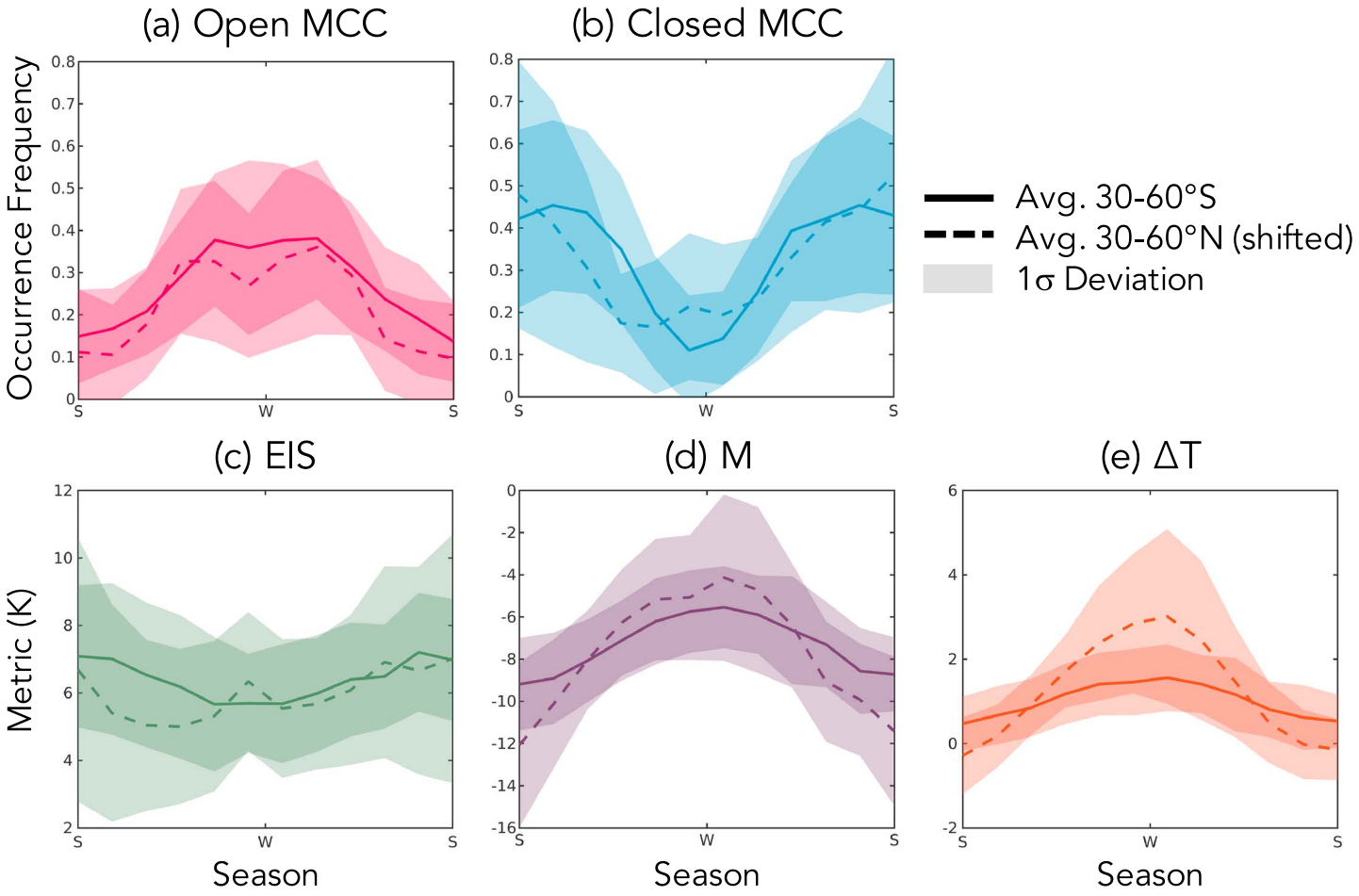

Figure 7. Seasonal cycles of midlatitude occurrence frequency for (a) open and (b) closed MCC clouds and the three meteorological control metrics: (c) EIS, (d) *M*, and (e) ΔT. Cloud frequencies and metric values are averaged across midlatitude bands (30–60°S, solid; 30–60°N, dashed). Combined spatial and submonthly 1σ standard deviations are included for reference (shading). NH seasonality has been shifted by 6 months to match SH (i.e., winter and summer are aligned). Midwinter lull, discussed in the text, occurs to the left of W in the NH.

exhibiting an equal dependence on EIS and ΔT. The highest f_{open} occurs at the largest *M* values (i.e., a stronger MCAO). These composites show that both low static stability and strong surface forcing favor open MCC clouds; *M* can capture both of those factors effectively. f_{closed} (Figure 8d) has a slightly weaker relationship with *M* (Figure 8b), depending more on EIS than ΔT. Closed MCC clouds are more frequent at weaker *M*, opposite to the open MCC cloud behavior (Figure 8c). This dependence on EIS is consistent with the seasonal cycle correlation coefficient map in Figure 6d showing a large region of correlation in the SEP and SEA for f_{closed}. As a result, the strong dependence on ΔT and *M* observed in the midlatitudes (Figure 7 and Table 1) is skewed toward EIS when the relationship is examined globally. Closed MCC clouds also tend to be sustained by longwave cloud top cooling more than by surface forcing, which may contribute to the smaller closed MCC cloud dependence on ΔT when regions of less prominent meteorological forcing are included (Shao & Randall, 1996; Wood, 2012; Wood et al., 2011).

Table 1
Seasonal Cycle Correlation Coefficients for Figure 7 Midlatitude Bands

	f_{open}			f_{closed}		
Regions	ML	NH	SH	ML	NH	SH
EIS	−0.60	*−0.57*	−0.94	0.77	0.72	0.91
M	0.91	0.94	0.98	−0.85	−0.94	−0.87
ΔT	0.79	0.92	0.98	−0.81	−0.92	−0.89

Note. Analysis performed using band averages for the NH (30–60°N), SH (30–60°S), and the combined NH and SH bands (ML). Italics indicate where correlations are insignificant at 95%.

Using the composite data from Figure 8, we can establish a functional dependence of f_{open} and f_{closed} on *M* (gray dots, Figures 9a and 9b). Parallel relationships can be developed between the mean binned EIS and ΔT and their associated frequencies, as shown in the supplement (gray dots, Figure S1). Examining these relationships with the composited EIS-ΔT data is especially enlightening as it shows the

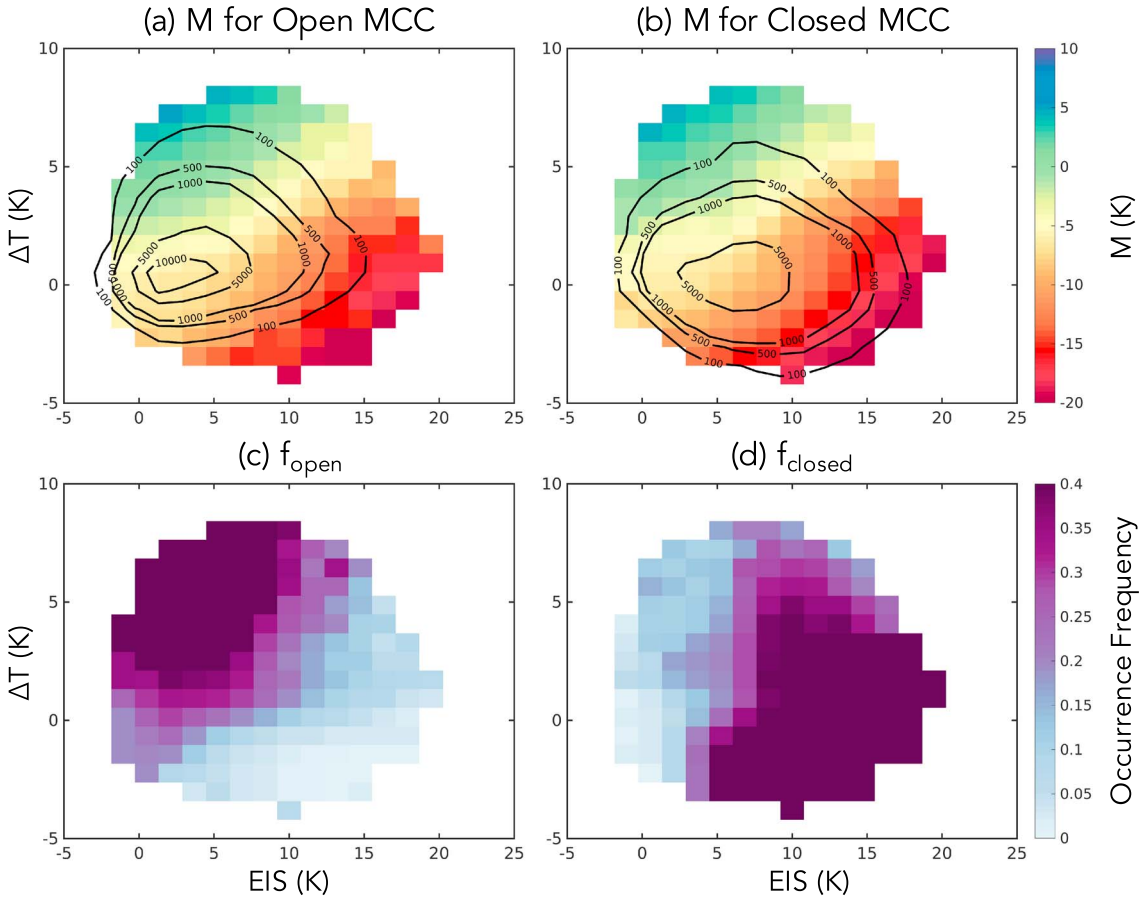

Figure 8. Two-dimensional composite histograms of M and occurrence frequency, respectively, for (a and c) open and (b and d) closed MCC clouds. Data are for all subscenes globally (65°S to 65°N) in 2008. The number of MCC cloud identifications (black contours in Figures 8a and 8b) indicates data spread in the histograms. Every histogram bin is required to have 50 or more identifications.

cloud behavior across a wide range of environmental and synoptic conditions (i.e., within a series of ranges of EIS and ΔT). This will clarify the relative importance of the three metrics. To quantify this importance, one can examine the strength of the correlation coefficients for the linear regression of these relationships (global values, Table 2). It is clear that the relationship between M and f_{open}, f_{closed} is significantly stronger than either EIS or ΔT with the frequencies. Furthermore, the relationship between M and f_{open} and f_{closed} is well described by a sigmoidal function (line in Figures 9a and 9b). The growth curve associated with f_{open} is strongly correlated to the binned data (Figure 9a, $R = +0.94$), while the decay curve associated with f_{closed} is slightly less correlated (Figure 9b, $R = -0.83$). A weaker correlation for f_{closed} compared to f_{open} is consistent with the stronger dependence on EIS seen in Figure 8d. Note that if one composites by M alone (line with shading for 2σ uncertainty in Figures 9a and 9b) the result is within the range of the composited data binned by EIS and ΔT (gray dots). The similarity between the two binning methods suggests robustness to the sigmoidal relationships between M and MCC cloud occurrence frequency. It also indicates that the MCC behavior is not obscured by the EIS-ΔT binning.

We can test our theory for the weaker global relationship between M and f_{closed} by repeating our histogram analysis for f_{closed} over a subset of regions (Figures 9d, S1b, and S1d): midlatitudes (black dots, 30–60°N and 30–60°S) and tropical (gold dots, 30°S to 30°N). The midlatitude f_{closed} has a good relation to M, slightly less scattered than the global relationship but similar (Figure 9d). f_{closed} in the tropics and subtropics have a much weaker relation to M and are far more scattered. This is consistent with the SEP and SEA regions being well correlated by EIS and minimally influenced by M and ΔT. The relationships between EIS, ΔT, and f_{closed} shown in Table 2 and Figures S1a and S1c confirm this as EIS dominates in the tropics over M and ΔT. f_{open} can be similarly analyzed in a subset of regions (Figures 9c, S1a, and S1c). Both the midlatitude and tropical

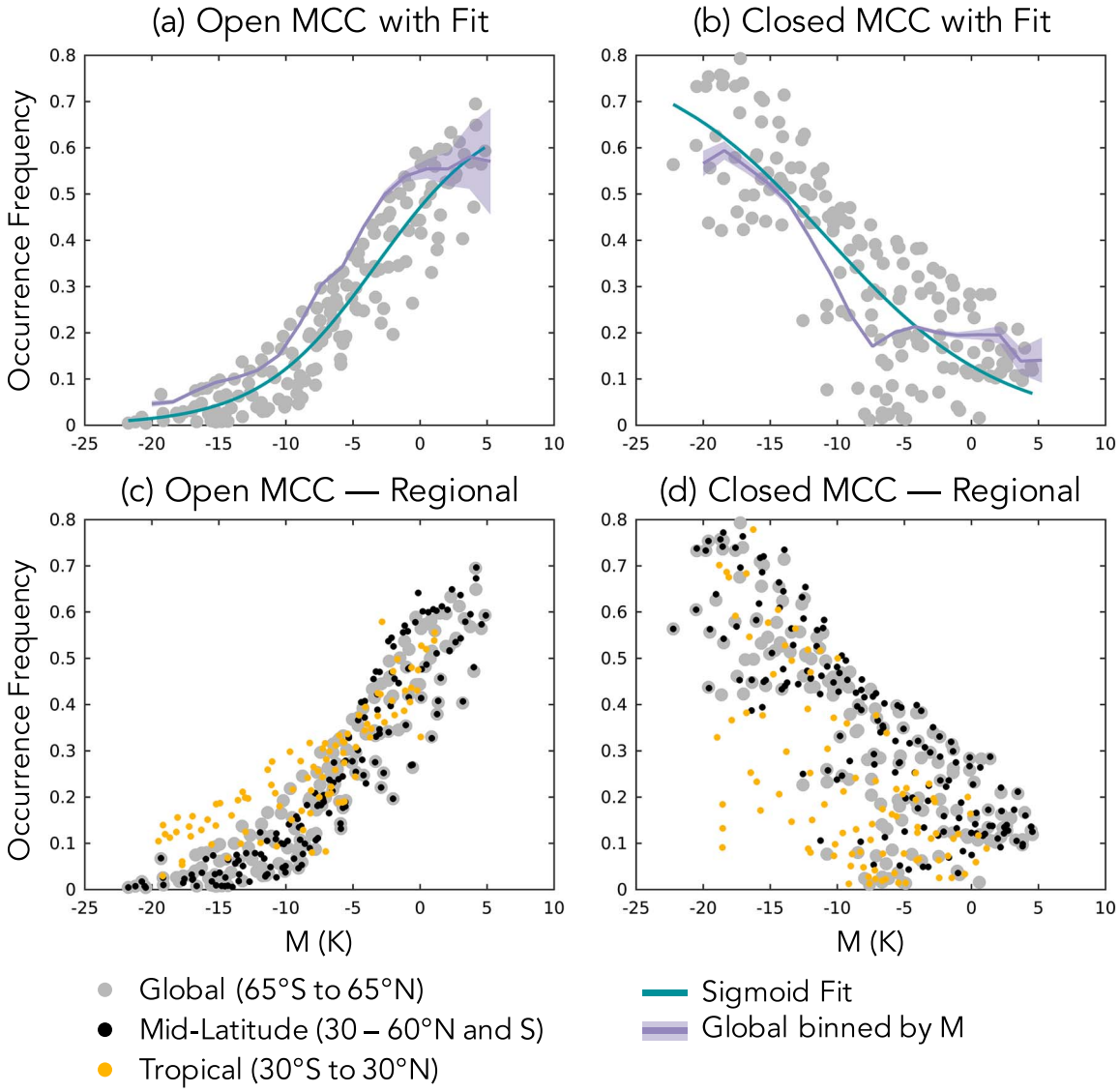

Figure 9. (a and b) Sigmoidal fits (line) of global composited data from Figure 8 (gray dots) for open and closed MCC clouds, respectively. Global data binned by *M* alone included for reference (line with shading for 2σ Poisson counting error). (c and d) ΔT-EIS composites computed for midlatitude (black) and tropical (gold) data are compared to global composite data (gray dots) for open and closed MCC clouds, respectively.

histogram results for f_{open} have strong relations to *M*. The subtropics and tropics show a slightly weaker relation and many more clouds occurring at lower *M*. This suggests that meteorology may be less important for open MCC cloud development in this region, consistent with research suggesting internal, precipitation associated mechanisms may be more important in these areas (e.g., Feingold et al., 2010; Savic-Jovcic & Stevens, 2008; Wood et al., 2011). For both open and closed MCC clouds, a large number of occurrences exist below $M = 0$ or -5 K. $M = 0$ K is often considered the cutoff for what is considered an MCAO event (Fletcher et al., 2016a, 2016b), although we have relaxed this definition to $M = -5$ K to encompass more low-cloud occurrences around MCAOs (discussed in the subsequent section and seen in Figure 3). The distinction between *M* as a metric for strong surface forcing and low stability instances and what is considered a technical MCAO event (strong *M* scenarios) is important to keep in mind.

Table 2
Correlation Coefficients for Regional EIS-ΔT Binned Data From Figures 9 and S1

	f_{open}			f_{closed}		
Regions	G	ML	T	G	ML	T
M	0.91	0.91	0.85	−0.81	−0.84	−0.63
ΔT	0.72	0.69	0.75	−0.51	−0.59	*0.12*
EIS	−0.62	−0.65	−0.53	0.74	0.68	0.88

Note. Regions analyzed are global (G, 65°S to 65°N), combined midlatitudes (ML, 30–60°N and S), and tropics (T, 30°S to 30°N). Italics indicate where correlations are insignificant at 95%.

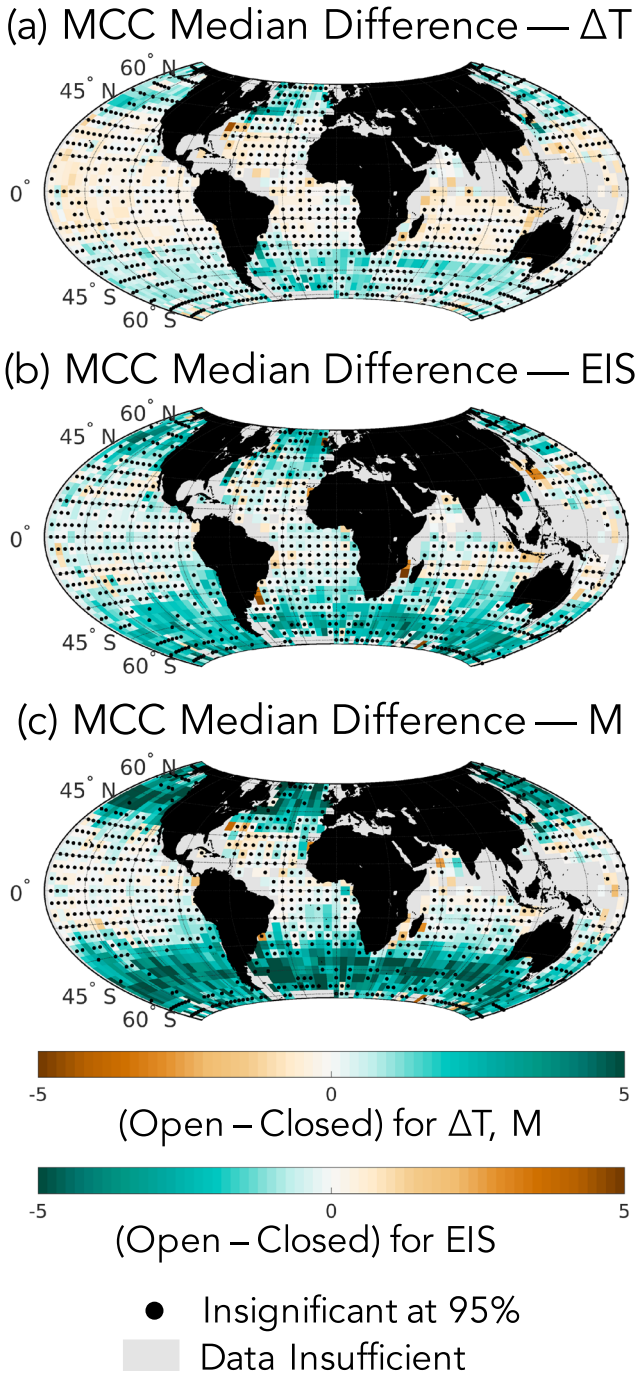

Figure 10. Means of monthly differences between the open and closed MCC cloud identified meteorological control metric distribution medians within each grid cell: (a) ΔT, (b) EIS, and (c) M. As in Figure 5, gray indicates regions of insufficient data. Dots denote where the distributions do not have significantly different medians at 95% confidence as tested by a Wilcoxen rank sum.

Is the predictive strength of the M-MCC cloud occurrence frequency relationship only due to the strong correlation between the seasonal cycle of cloud occurrence and metric values? We can demonstrate that there is a strong connection on a shorter time scale (i.e., with the seasonal cycle removed) by looking at the monthly PDF median difference between the metric values for open and closed MCC clouds and averaging the differences over the full year (shown in Figures 10a–10c respectively for EIS, ΔT, and M). That is, in every $5 \times 5°$ grid box the median of the monthly metric PDF has been computed for open and closed MCC clouds and differenced. The annual average of the monthly median difference is then computed (Figure 10). The significance of this difference (i.e., whether or not the medians are separated statistically for the range of the metric) is tested with a Wilcoxen rank sum or Mann-Whitney U test. Bins that have failed the significance test at 95% confidence (e.g., their PDFs overlap making the difference nonsignificant) are marked with a black dot in Figure 10. The seasonal cycle of the data is effectively removed by computing the differences monthly and then averaging the result over the year. Thus, significant differences denote the separation of open and closed MCC cloud metric values on short time scales. The results show that M is superior to the other metrics tested in distinguishing open and closed MCC clouds on subseasonal time scales. This superiority has two sources: (1) M has the largest separation in value between open and closed MCC clouds (color in Figure 10c) and (2) M shows the most grid boxes with statistically significant separation between the average open and closed values (fewest dots or test failures in Figure 10c). All plots are on the same temperature scale, −5 to 5 K, clearly showing the magnitude of separation for each metric. The metrics have very different scales, however, so the separation must be considered alongside the significance test results. The strongest and most statistically significant separation of open and closed MCC cloud occurs for M in the midlatitudes. Comparing all metrics across the two latitude bands of 30–60°N and S, there are a total of 160 grid boxes that are significant for ΔT (Figure 10a), 257 for EIS (Figure 10b), and 332 for M (Figure 10c). The separation between open and closed values of M is not statistically significant over the tropical region, as expected due to the differing dynamics and mechanisms that exist there. Interestingly, ΔT has the most statistically significant points in the tropics. The direction of the ΔT difference also switches between open and closed MCC clouds in this region. We can conclude from the analysis in this section that M is the best of the three metrics at distinguishing between open and closed MCC clouds in latitudes poleward of 30°N and S at short time scales.

3.4. Composites of MCAO and MCC Cloud Environments

In the previous sections of this paper, we have shown that the MCAO index, M, is a good predictor of MCC cloud occurrence frequency. There is an especially strong relationship of M to open MCC clouds. Thus far we have examined these clouds and their relationships in a static framework, through snapshots of cloud occurrence and associated meteorology. These systems are very dynamic, however, with clouds evolving in time through the influence of MCAOs. How well is M able to capture the Lagrangian evolution of these clouds? While the bulk of this question will be answered in subsequent work, a preliminary answer can be found by compositing the MCC cloud occurrence data around MCAO events (Figure 11). Composites of three NNA identification cloud types are shown in Figure 11 for the full year of data in the Northern (30–60°N) and Southern (30–60°S) hemispheres, respectively: closed MCC (a and d), open MCC (b and e), and cellular but disorganized clouds (c and f). MCAO events are identified as contiguous

regions having $M > -5$ K. As previously discussed, this is a relaxed limit compared to the typical definition of a MCAO event when $M \geq 0$ K (marking the strongest of outbreaks). The choice of $M = -5$ K is more inclusive of low-cloud occurrences around the cold air outbreak (Fletcher et al., 2016a, 2016b). Our reasoning is guided by the results in Figures 8 and 9 showing a significant portion of open MCC clouds occurring below $M = 0$ K before dropping off below $M = -5$ K. Closed MCC clouds are also numerous between $M = 0$ and -5 K. As we are interested in capturing the evolution of these cloud types, it is important not to over restrict the cases examined. Additionally, our MCAO composite analysis is qualitative so the choice of MCAO event cut off can be more flexible. When compositing around these events, the grid point where M is a maximum within the closed contour of $M \geq -5$ K is chosen as the center MCAO and positioned at the composite origin (as in Fletcher et al., 2016a). The composite mean location of $M = -5$ K is also shown (dashed line). For reference, contours of composite sea level pressure are overlaid.

Examining the MCC cloud evolution along the mean flow (arrows in Figure 11, as deduced from sea level pressure contours assuming near geostrophic wind balance) in these composites is a reasonable proxy for Lagrangian evolution of MCC clouds around MCAOs. Note that the SLP contours are not streamlines so this is not the exact time evolution of the clouds but an approximation. High stability over high-latitude oceans drives extensive low cloud, frequently of the closed MCC cloud form and occasionally, with the right shearing wind conditions, roll cloud (Atkinson & Zhang, 1996; Fletcher et al., 2016a, 2016b). Marine cold air outbreaks begin over cold surface temperatures (tail of arrow, Figures 11g and 11h), before heading equatorward and pulling these low clouds along over warmer SST. Indeed, Figures 11a and 11d show the highest frequency of closed MCC clouds at the start of the flow (top in a, bottom in d). Roll clouds are identified by the NNA as closed MCC clouds, so this includes both cases. The MCAO advects the clouds over progressively warmer water as it heads to the equator, transitioning closed to open MCC clouds (Abel et al., 2017; Atkinson & Zhang, 1996; Fletcher et al., 2016b; Wyant et al., 1997). Open MCC clouds are most frequent in the center of the composites in Figures 11b and 11e, slightly to the east of the mean center of the MCAO event and consistent with the flow traced from the SLP contours. The f_{open} maximum occurs slightly downstream from the peak M values in the Lagrangian perspective, intriguingly. This is consistent with results found in Fletcher et al. (2016a) for composites of ERA-Interim planetary boundary layer (PBL) height around stronger MCAOs ($M > 6$ K instead of -5 K). They found that a minimum in PBL height occurred far upstream of the M maximum (where closed MCC clouds would occur) and a maximum in PBL height about 200–500 km downstream of the maximum in M (where we see open MCC clouds) (Fletcher et al., 2016a). This could be an indication that time is needed for the development of open MCC clouds (i.e., that they need to be advected beyond the peak M that influenced them before developing sufficiently). Finally, as the flow continues to move the clouds toward the equator, the open MCC clouds will continue to evolve into aggregated cumulus cloud which is captured by the cellular but disorganized cloud category of the NNA. This final transition is seen more clearly in the SH (Figure 11f) but still exists in the NH (Figure 11c). A larger amount of cumulus and other disorganized clouds occur in the NH than the SH relative to the other types shown, obscuring the final stage of the transition. The MCAO composites in Figure 11 show that the evolution of open and closed MCC clouds is influenced by MCAO events consistent with theory.

An intriguing and yet unexplored discovery was made about the environment that open and closed MCC clouds occur within. Along with the meteorological differences illustrated previously, open and closed MCC clouds have very different large-scale vertical velocities (measured in pressure coordinates as ω_{700}, Figure 12a). Zonally averaged annual mean values of ω_{700} are generally more positive for open MCC clouds than closed, indicating larger subsidence in the environment of those clouds. In the subtropics and tropics, open MCC clouds are weakly subsiding or without significant vertical wind. This overlaps with the weakly subsiding or strongly ascending closed MCC clouds seen in those areas. In the midlatitudes, along with greater subsidence, open MCC clouds have more positive values of M than closed MCC clouds as we showed earlier in Figure 10. For comparison purposes, M has been plotted similar to ω_{700} in Figure 12b. The connection between regions of stronger M values and more subsidence indicates large-scale dynamics at work in MCAO. This is consistent with the descending air, known as the dry intrusion or airstream, typically found on the cold side of cyclones (Catto, 2016; Field & Wood, 2007; Schultz, 2001). It is remarkable that open cells are associated with both weak static stability and strong subsidence. Berner et al. (2013) showed that subsidence can suppress transition from closed to open cells, making this finding somewhat counterintuitive and

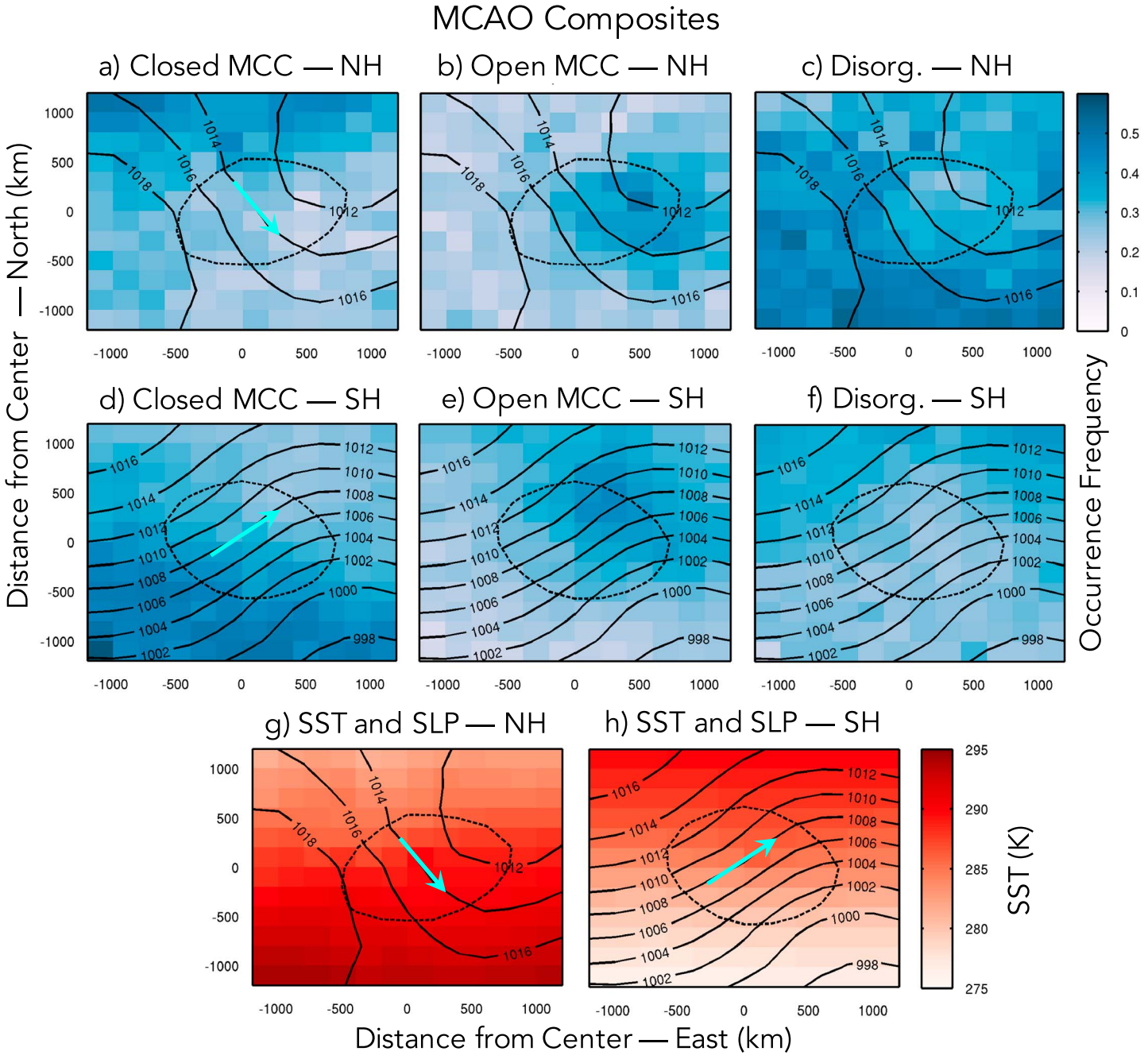

Figure 11. Composites of (a and d) closed MCC, (b and e) open MCC, and (c and f) cellular but disorganized cloud occurrence frequency; and (g and h) surface temperature around MCAO events ($M \geq -5$ K). Sea level pressure contours are included for reference. As in Figure 3, mean flow arrows are sketched assuming approximate geostrophic balance (Figures 11a, 11d, 11g, and 11h). Lagrangian evolution of clouds approximately follows MCAO flow (arrows) from high to low latitudes over warming water (Figures 11g and 11h). NH (30–60°N, Figures 11a–11c) and SH (30–60°S, Figures 11d–11f) composited separately. When an MCAO event is identified, MCC cloud subscenes occurring within 3 h of the event and within 2000 km of the MCAO center are identified. The location of the MCC cloud subscene relative to MCAO center is identified on an equal area grid, and the frequency with which each MCC cloud type occurs in each grid box (bin size 200 × 200 km) is calculated. *M*, surface temperature, and sea level pressure derived from ERA-Interim are interpolated to the same equal area grid (200 × 200 km) prior to compositing. Times during which an MCAO event is identified, but for which there is no corresponding MCC cloud subscene, are not included in the ERA-Interim data compositing.

worthy of future explanation. The source of subsidence, mechanics of its influence on open and closed MCC clouds, and the evolution of open and closed MCC clouds with MCAO will be investigated with the help of Lagrangian trajectories in the future.

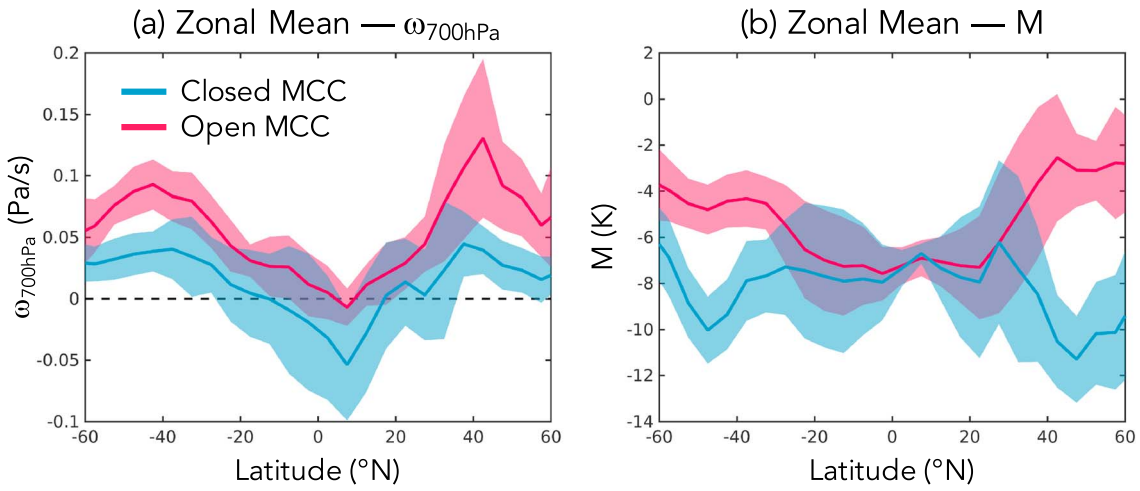

Figure 12. Zonally averaged (a) ω_{700} and (b) M over monthly means (line) with 1σ standard deviation (shading). Subsidence is defined as positive ω_{700} (see dashed zero-line for reference).

4. Summary and Discussion

We set out to test the hypothesis that the frequency of occurrence of open MCC cloud is strongly tied to cold air outbreaks and that a simple metric can be used to predict MCC cloud occurrence. Three metrics were chosen to represent the key influences on development: M, the marine cold air outbreak index; EIS, estimated inversion strength; and ΔT, sea-air temperature difference.

We discovered several important aspects of open and closed MCC structure, radiative impacts, and formation mechanisms. These are as follows:

First, open and closed MCC clouds have distinct cloud fraction-albedo relations, such that the structure and microphysical properties of open and closed MCC clouds are sufficiently different that the same fractional cloud coverage yields a different optical depth and albedo. Closed MCC cloud, for a given cloud fraction, tends to have a higher albedo than open MCC cloud except at very high cloud fractions. The CF-albedo relationships show that prediction of open and closed MCC based on cloud fraction alone will be insufficient as it cannot capture the complex MCC cloud morphology.

Second, open and closed MCC clouds have a well-defined geographic distribution and strong seasonality. Closed MCC clouds occur in the cold Eastern subtropical oceans and over summertime midlatitude oceans, while open MCC clouds are widespread globally, as in Muhlbauer et al. (2014). The seasonal cycle of open MCC cloud is best correlated with the MCAO index. A strong connection between outbreaks and open MCC cloud development in the midlatitudes is found, consistent with the literature (Agee, 1987; Atkinson & Zhang, 1996; Muhlbauer et al., 2014; Wood, 2012). The seasonal cycle of closed MCC cloud is well correlated with M in the midlatitudes and EIS in the subtropics (specifically SEA and SEP), consistent with previous studies (Wood & Hartmann, 2006).

Third, M is a superior predictor of open MCC cloud occurrence largely because the MCAO index better encompasses both surface forcing and static instability. Surface forcing has been previously established as a driver of open MCC cloud development (Kazil et al., 2014); we find that static instability is favorable to open MCC cloud as well. Strong sigmoidal relationships were found between M and occurrence frequency of open and closed MCC clouds. Open MCC cloud occurrence frequency grows strongly with M in all regions. M is a slightly weaker predictor for closed MCC cloud globally because of the cloud type's stronger dependence on EIS over ΔT in the tropics. Of the metrics tested, M is also the best discriminator between occurrence of open and closed MCC clouds on sub seasonal time scales.

Fourth, open and closed MCC clouds evolve with MCAO events. Composites of MCC around MCAO events indicate that MCAOs from regions of cold surface temperature off high-latitude ice and land drive a transition from closed to open MCC clouds and then to cellular but disorganized clouds as they progress equatorward over warmer ocean. Midlatitude and tropical open MCC clouds tend to occur in more strongly subsiding

environments than closed MCC clouds. This may be connected to the dynamics of MCAO events and will be investigated in the future using Lagrangian trajectories.

Our results have interesting implications for cloud feedbacks. Much of the research on cloud feedbacks and improving model predictions uses fractional cloud cover as a way of quantifying cloud radiative influence. It is highly probable that cloud cover will change with global warming. Metrics like estimated inversion strength (EIS) (Wood & Bretherton, 2006) and sea surface temperature (SST) predict low-cloud cover in observations of the current climate and in GCM-simulated present and future climates (Clement et al., 2009; Myers & Norris, 2015, 2016; Norris et al., 2016; Qu et al., 2014, 2015; Seethala et al., 2015). The magnitude of change in low-cloud cover is still uncertain in GCMs (Qu et al., 2014, 2015). However, they all indicate that cloud cover will reduce with global warming thus constituting a positive feedback. Kolstad and Bracegirdle (2008) found that MCAO's in the Northern Hemisphere are predicted to weaken in strength with global warming, although their frequency stays the same. A weakening would yield a reduction in the magnitude of M in the NH and, provided one can extend these results, in the SH. If we assume that MCAOs are affected in both hemispheres and that our closed and open MCC cloud relations with M (Figure 9) are invariant in a warmed climate, this would suggest that in the future there may be less open MCC cloud and more closed MCC cloud in the middle and high latitudes. If we further assume that the cloud fraction-albedo relations (Figure 4) are invariant in a warmed climate, this transition between low-cloud states (i.e., more open to more closed MCC clouds occurring) suggests that we would have a shift from lower albedo clouds to higher albedo clouds. This would constitute a negative cloud feedback and would be important given the coverage and frequency of these MCC clouds. A decrease in cloud cover *and* an increase in closed MCC cloud occurrence frequency are not mutually exclusive as we have shown that closed MCC clouds exist for a range of cloud fractions. In this instance, we could have more closed MCC clouds (with higher albedo) but lower cloud fraction (consistent with model predictions). The feedback from a shift in MCC type driven by MCAO weakening would change the degree of positive feedback expected from a decrease in cloud cover.

In discussing our theory for a MCC Cloud Feedback, it is important to recognize the limitation of not knowing the invariance of open and closed MCC cloud relationships under climate change. We expect some robustness of the f_{MCC}-M (Figure 9) and CF-albedo (Figure 4) curves since we have included many different climatological states in our analysis. The clouds sampled in our study have occurred over a broad range of CF, meteorological regime, and SST. However, this is not to say that the curves will not change as they may not be completely invariant to all manifestations of climate change. For example, changes in atmospheric emissivity may affect both the f_{MCC}-M and CF-albedo curves found for open and closed MCC clouds in the present climate. Increased downwelling longwave (LW) with increased CO_2 will act to suppress LW cloud top cooling, an important element for sustaining closed MCC clouds (Shao & Randall, 1996). One would expect that reduced cooling would be a less conducive environment for closed MCC clouds, manifesting as a lower frequency of closed MCC clouds and/or higher frequency of transition state clouds. Along with affecting the f_{MCC}-M relations (Figure 9), the cloud fraction of closed MCC clouds could be adversely affected from suppression of cloud top cooling which would additionally alter the CF-albedo curves (Figure 4). It is unclear at this point how important LW cloud top cooling is to either of these relationships, but this example serves to demonstrate a potential lack of invariance that will introduce a structural uncertainty into our analysis. This is an issue that many other analyses have encountered when using present day observations of clouds to understand their future behavior under climate change (McCoy et al., 2017; Myers & Norris, 2015, 2016; Qu et al., 2015). Following the methodology of these earlier works, appropriate usage of interannual observations and GCM behaviors can be used to quantify the MCC Cloud Feedback, caused by a transition between low-cloud states, and reduce its structural uncertainties. As MCC clouds can significantly impact the climate system, understanding their behavior under global warming will be very worthwhile.

Acknowledgments
We acknowledge the Level 1 and Atmosphere Archive and Distribution System (LAADS) Distributed Active Archive Center (DAAC) for NASA MODIS data used in the neural network (obtained at https://ladsweb.modaps.eosdis.nasa.gov/); the NASA Langley Research Center Atmospheric Science Data Center (ASDC) for CERES data (https://ceres.larc.nasa.gov); and the NOAA Oceanic and Atmospheric Research (OAR) Earth System Research Laboratory (ESRL) Physical Sciences Division (PSD) for the OI SST V2 data (http://www.esrl.noaa.gov/psd/). We thank Ryan Eastman for providing ECMWF ERA-Interim Reanalysis data (http://apps.ecmwf.int/datasets/data/interim-full-daily/) and insight. Additionally, we wish to acknowledge the invaluable discussions and support of Daniel McCoy and Chris Bretherton throughout this process. This manuscript was improved thanks to the numerous suggestions and comments of Tim Myers and two anonymous reviewers as well as the editing expertise of Minghua Zhang. McCoy acknowledges funding for this work from the American Meteorological Society Graduate Fellowship and the National Science Foundation Graduate Fellowship Program (grant: DGE-1256082). Additional funding was provided by NASA award NNX13AQ35G.

References

Abel, S. J., Boutle, I. A., Waite, K., Fox, S., Brown, P. R. A., Cotton, R., … Bower, K. N. (2017). The role of precipitation in controlling the transition from stratocumulus to cumulus clouds in a Northern Hemisphere cold-air outbreak. *Journal of the Atmospheric Sciences*, *74*(7), 2293–2314. https://doi.org/10.1175/jas-d-16-0362.1

Ackerman, S. A., Holz, R. E., Frey, R., Eloranta, E. W., Maddux, B. C., & McGill, M. (2008). Cloud detection with MODIS. Part II: Validation. *Journal of Atmospheric and Oceanic Technology*, *25*(7), 1073–1086. https://doi.org/10.1175/2007jtecha1053.1

Ackerman, S. A., Strabala, K., Menzel, P., Frey, R., Moeller, C., Gumley, L., … Zhang, H. (2002). Discriminating clear-sky from cloud with MODIS algorithm theoretical basis document (MOD35)Rep., NASA.

Agee, E. M. (1984). Observations from space and thermal-convection: A historical perspective. *Bulletin of the American Meteorological Society*, *65*(9), 938–949. https://doi.org/10.1175/1520-0477(1984)065%3C0938:ofsatc%3E2.0.co;2

Agee, E. M. (1987). Mesoscale cellular convection over the oceans. *Dynamics of Atmospheres and Oceans*, *10*(4), 317–341. https://doi.org/10.1016/0377-0265(87)90023-6

Agee, E. M., Chen, T. S., & Dowell, K. E. (1973). Review of mesoscale cellular convection. *Bulletin of the American Meteorological Society*, *54*(10), 1004–1012. https://doi.org/10.1175/1520-0477(1973)054%3C1004:aromcc%3E2.0.co;2

Atkinson, B. W., & Zhang, J. W. (1996). Mesoscale shallow convection in the atmosphere. *Reviews of Geophysics*, *34*(4), 403–431. https://doi.org/10.1029/96RG02623

Bénard, H. (1901). Les tourbillons cellulaires dans une nappe liquide—Méthodes optiques d'observation et d'enregistrement. *Journal of Physics, Theoretical and Applied*, *10*(1), 254–266. https://doi.org/10.1051/jphystap:0190100100025400

Bender, F. A. M., Charlson, R. J., Ekman, A. M. L., & Leahy, L. V. (2011). Quantification of monthly mean regional-scale albedo of marine stratiform clouds in satellite observations and GCMs. *Journal of Applied Meteorology and Climatology*, *50*(10), 2139–2148. https://doi.org/10.1175/jamc-d-11-049.1

Bender, F. A. M., Engstroem, A., Wood, R., & Charlson, R. J. (2017). Evaluation of hemispheric asymmetries in marine cloud radiative properties, *Journal of Climate, 30*, 4131–4147.

Bender, F. A. M., Engstrom, A., & Karlsson, J. (2016). Factors controlling cloud albedo in marine subtropical stratocumulus regions in climate models and satellite observations. *Journal of Climate*, *29*(10), 3559–3587. https://doi.org/10.1175/jcli-d-15-0095.1

Bennartz, R. (2007). Global assessment of marine boundary layer cloud droplet number concentration from satellite. *Journal of Geophysical Research*, *112*, D02201. https://doi.org/10.1029/2006JD007547

Bennartz, R., Shupe, M. D., Turner, D. D., Walden, V. P., Steffen, K., Cox, C. J., … Pettersen, C. (2013). July 2012 Greenland melt extent enhanced by low-level liquid clouds. *Nature*, *496*(7443), 83–86. https://doi.org/10.1038/nature12002

Berner, A. H., Bretherton, C. S., Wood, R., & Muhlbauer, A. (2013). Marine boundary layer cloud regimes and POC formation in a CRM coupled to a bulk aerosol scheme. *Atmospheric Chemistry and Physics*, *13*(24), 12,549–12,572. https://doi.org/10.5194/acp-13-12549-2013

Bodas-Salcedo, A., Hill, P. G., Furtado, K., Williams, K. D., Field, P. R., Manners, J. C., & Hyder, P. (2016). Large contribution of supercooled liquid clouds to the solar radiation budget of the Southern Ocean. *Journal of Climate*, *29*(11), 4213–4228. https://doi.org/10.1175/jcli-d-15-0564.1

Bodas-Salcedo, A., Williams, K. D., Field, P. R., & Lock, A. P. (2012). The surface downwelling solar radiation surplus over the Southern Ocean in the Met Office Model: The role of midlatitude cyclone clouds. *Journal of Climate*, *25*(21), 7467–7486. https://doi.org/10.1175/jcli-d-11-00702.1

Boers, R., & Mitchell, R. M. (1994). Absorption feedback in stratocumulus clouds influence on cloud top albedo. *Tellus A*, *46*(3), 229–241. https://doi.org/10.1034/j.1600-0870.1994.00001.x

Boucher, O., Randall, D., Artaxo, P., Bretherton, C., Feingold, G., Forster, P., … Zhang, X.Y. (2013). *Clouds and aerosols Rep*. Cambridge, UK and New York: Cambridge University Press.

Bretherton, C. S., & Wyant, M. C. (1997). Moisture transport, lower-tropospheric stability, and decoupling of cloud-topped boundary layers. *Journal of the Atmospheric Sciences*, *54*(1), 148–167. https://doi.org/10.1175/1520-0469(1997)054%3C0148:mtltsa%3E2.0.co;2

Brummer, B. (1996). Boundary-layer modification in wintertime cold-air outbreaks from the Arctic sea ice. *Boundary Layer Meteorology*, *80*(1-2), 109–125. https://doi.org/10.1007/bf00119014

Catto, J. L. (2016). Extratropical cyclone classification and its use in climate studies. *Reviews of Geophysics*, *54*, 486–520. https://doi.org/10.1002/2016RG000519

Clement, A. C., Burgman, R., & Norris, J. R. (2009). Observational and model evidence for positive low-level cloud feedback. *Science*, *325*(5939), 460–464. https://doi.org/10.1126/science.1171255

Dee, D. P., Uppala, S. M., Simmons, A. J., Berrisford, P., Poli, P., Kobayashi, S., … Vitart, F. (2011). The ERA-Interim reanalysis: Configuration and performance of the data assimilation system. *Quarterly Journal of the Royal Meteorological Society*, *137*(656), 553–597. https://doi.org/10.1002/qj.828

Engstrom, A., Bender, F. A. M., Charlson, R. J., & Wood, R. (2015). The nonlinear relationship between albedo and cloud fraction on near-global, monthly mean scale in observations and in the CMIP5 model ensemble. *Geophysical Research Letters*, *42*, 9571–9578. https://doi.org/10.1002/2015GL066275

Engstrom, A., Bender, F. A. M., & Karlsson, J. (2014). Improved representation of marine stratocumulus cloud shortwave radiative properties in the CMIP5 climate models. *Journal of Climate*, *27*(16), 6175–6188. https://doi.org/10.1175/jcli-d-13-00755.1

Feingold, G., Koren, I., Wang, H., Xue, H., & Brewer, W. A. (2010). Precipitation-generated oscillations in open cellular cloud fields. *Nature*, *466*(7308), 849–852. http://www.nature.com/nature/journal/v466/n7308/abs/nature09314.html#supplementary-information. https://doi.org/10.1038/nature09314

Field, P. R., Bodas-Salcedo, A., & Brooks, M. E. (2011). Using model analysis and satellite data to assess cloud and precipitation in midlatitude cyclones. *Quarterly Journal of the Royal Meteorological Society*, *137*(659), 1501–1515. https://doi.org/10.1002/qj.858

Field, P. R., Cotton, R. J., McBeath, K., Lock, A. P., Webster, S., & Allan, R. P. (2014). Improving a convection-permitting model simulation of a cold air outbreak. *Quarterly Journal of the Royal Meteorological Society*, *140*(678), 124–138. https://doi.org/10.1002/qj.2116

Field, P. R., & Wood, R. (2007). Precipitation and cloud structure in midlatitude cyclones. *Journal of Climate*, *20*(2), 233–254. https://doi.org/10.1175/jcli3998.1

Fletcher, J., Mason, S., & Jakob, C. (2016a). The climatology, meteorology, and boundary layer structure of marine cold air outbreaks in both hemispheres*. *Journal of Climate*, *29*(6), 1999–2014. https://doi.org/10.1175/jcli-d-15-0268.1

Fletcher, J. K., Mason, S., & Jakob, C. (2016b). A climatology of clouds in marine cold air outbreaks in both hemispheres. *Journal of Climate*, *29*(18), 6677–6692. https://doi.org/10.1175/jcli-d-15-0783.1

Forbes, R. M., & Ahlgrimm, M. (2014). On the representation of high-latitude boundary layer mixed-phase cloud in the ECMWF global model. *Monthly Weather Review*, *142*(9), 3425–3445. https://doi.org/10.1175/mwr-d-13-00325.1

George, R. C., & Wood, R. (2010). Subseasonal variability of low cloud radiative properties over the southeast Pacific Ocean. *Atmospheric Chemistry and Physics*, *10*(8), 4047–4063. https://doi.org/10.5194/acp-10-4047-2010

Graham, A. (1934). Shear patterns in an unstable layer of air. *Philosophical Transactions of the Royal Society of London, Series A, Containing Papers of a Mathematical or Physical Character*, *232*(707-720), 285–296. https://doi.org/10.1098/rsta.1934.0008

Grosvenor, D. P., & Wood, R. (2014). The effect of solar zenith angle on MODIS cloud optical and microphysical retrievals within marine liquid water clouds. *Atmospheric Chemistry and Physics*, *14*(14), 7291–7321. https://doi.org/10.5194/acp-14-7291-2014

Gufan, A., Lehahn, Y., Fredj, E., Price, C., Kurchin, R., & Koren, I. (2016). Segmentation and tracking of marine cellular clouds observed by geostationary satellites. *International Journal of Remote Sensing*, *37*(5), 1055–1068. https://doi.org/10.1080/2150704x.2016.1142681

Hartmann, D. L. (2016). *Global physical climatology* (2nd ed.). Amsterdam, Netherlands: Elsevier.

Hartmann, D. L., & Short, D. A. (1980). On the use of Earth radiation budget statistics for studies of clouds and climate. *Journal of the Atmospheric Sciences*, *37*(6), 1233–1250. https://doi.org/10.1175/1520-0469(1980)037%3C1233:otuoer%3E2.0.co;2

Kay, J. E., Wall, C., Yettella, V., Medeiros, B., Hannay, C., Caldwell, P., & Bitz, C. (2016). Global climate impacts of fixing the Southern Ocean shortwave radiation bias in the Community Earth System Model (CESM). *Journal of Climate*, *29*(12), 4617–4636. https://doi.org/10.1175/jcli-d-15-0358.1

Kazil, J., Feingold, G., Wang, H., & Yamaguchi, T. (2014). On the interaction between marine boundary layer cellular cloudiness and surface heat fluxes. *Atmospheric Chemistry and Physics*, *14*(1), 61–79. https://doi.org/10.5194/acp-14-61-2014

King, M. D., Menzel, W. P., Kaufman, Y. J., Tanre, D., Gao, B. C., Platnick, S., … Hubanks, P. A. (2003). Cloud and aerosol properties, precipitable water, and profiles of temperature and water vapor from MODIS. *IEEE Transactions on Geoscience and Remote Sensing*, *41*(2), 442–458. https://doi.org/10.1109/tgrs.2002.808226

Klein, S. A., & Hartmann, D. L. (1993). The seasonal cycle of low stratiform clouds. *Journal of Climate*, *6*(8), 1587–1606. https://doi.org/10.1175/1520-0442(1993)006%3C1587:tscols%3E2.0.co;2

Kolstad, E. W., & Bracegirdle, T. J. (2008). Marine cold-air outbreaks in the future: An assessment of IPCC AR4 model results for the Northern Hemisphere. *Climate Dynamics*, *30*(7-8), 871–885. https://doi.org/10.1007/s00382-007-0331-0

Kolstad, E. W., Bracegirdle, T. J., & Seierstad, I. A. (2009). Marine cold-air outbreaks in the North Atlantic: Temporal distribution and associations with large-scale atmospheric circulation. *Climate Dynamics*, *33*(2-3), 187–197. https://doi.org/10.1007/s00382-008-0431-5

Leslie, J. (2017). NOAA's GOES-16 satellite sends first images to Earth. In K. Hille (Ed.).

Loeb, N. G., Wielicki, B. A., Rose, F. G., & Doelling, D. R. (2007). Variability in global top-of-atmosphere shortwave radiation between 2000 and 2005. *Geophysical Research Letters*, *34*, L03704. https://doi.org/10.1029/2006GL028196

Ma, X. L., Wan, Z., Moeller, C. C., Menzel, W. P., Gumley, L. E., & Zhang, Y. (2000). Retrieval of geophysical parameters from moderate resolution imaging spectroradiometer thermal infrared data: Evaluation of a two-step physical algorithm. *Applied Optics*, *39*(20), 3537–3550. https://doi.org/10.1364/AO.39.003537

McCoy, D. T., Eastman, R., Hartmann, D. L., & Wood, R. (2017). The change in low cloud cover in a warmed climate inferred from AIRS, MODIS, and ERA-interim. *Journal of Climate*, *30*(10), 3609–3620. https://doi.org/10.1175/jcli-d-15-0734.1

McCoy, D. T., Tan, I., Hartmann, D. L., Zelinka, M. D., & Storelvmo, T. (2016). On the relationships among cloud cover, mixed-phase partitioning, and planetary albedo in GCMs. *Journal of Advances in Modeling Earth Systems*, *8*(2), 650–668. https://doi.org/10.1002/2015MS000589

Morrison, H., de Boer, G., Feingold, G., Harrington, J., Shupe, M. D., & Sulia, K. (2012). Resilience of persistent Arctic mixed-phase clouds. *Nature Geoscience*, *5*(1), 11–17.

Muhlbauer, A., McCoy, I. L., & Wood, R. (2014). Climatology of stratocumulus cloud morphologies: Microphysical properties and radiative effects. *Atmospheric Chemistry and Physics*, *14*(13), 6695–6716. https://doi.org/10.5194/acp-14-6695-2014

Muller, G., & Chlond, A. (1996). Three-dimensional numerical study of cell broadening during cold-air outbreaks. *Boundary Layer Meteorology*, *81*(3-4), 289–323. https://doi.org/10.1007/bf02430333

Myers, T. A., & Norris, J. R. (2015). On the relationships between subtropical clouds and meteorology in observations and CMIP3 and CMIP5 models. *Journal of Climate*, *28*(8), 2945–2967. https://doi.org/10.1175/JCLI-D-14-00475.1

Myers, T. A., & Norris, J. R. (2016). Reducing the uncertainty in subtropical cloud feedback. *Geophysical Research Letters*, *43*, 2144–2148. https://doi.org/10.1002/2015GL067416

Nakamura, H. (1992). Midwinter suppression of baroclinic wave activity in the Pacific. *Journal of the Atmospheric Sciences*, *49*(17), 1629–1642. https://doi.org/10.1175/1520-0469(1992)049%3C1629:MSOBWA%3E2.0.CO;2

Naud, C. M., Booth, J. F., & Del Genio, A. D. (2014). Evaluation of ERA-Interim and MERRA cloudiness in the Southern Ocean. *Journal of Climate*, *27*(5), 2109–2124. https://doi.org/10.1175/jcli-d-13-00432.1

Naud, C. M., Booth, J. F., & Del Genio, A. D. (2016). The relationship between boundary layer stability and cloud cover in the post-cold-frontal region. *Journal of Climate*, *29*(22), 8129–8149. https://doi.org/10.1175/jcli-d-15-0700.1

Norris, J. R., Allen, R. J., Evan, A. T., Zelinka, M. D., O'Dell, C. W., & Klein, S. A. (2016). Evidence for climate change in the satellite cloud record. *Nature*, *536*, 72–75. https://doi.org/10.1038/nature18273

Painemal, D., & Zuidema, P. (2011). Assessment of MODIS cloud effective radius and optical thickness retrievals over the Southeast Pacific with VOCALS-REx in situ measurements. *Journal of Geophysical Research*, *116*, D24206. https://doi.org/10.1029/2011JD016155

Papritz, L., Pfahl, S., Sodemann, H., & Wernli, H. (2015). A climatology of cold air outbreaks and their impact on air–sea heat fluxes in the high-latitude South Pacific. *Journal of Climate*, *28*(1), 342–364. https://doi.org/10.1175/JCLI-D-14-00482.1

Penny, S., Roe, G. H., & Battisti, D. S. (2010). The source of the midwinter suppression in storminess over the North Pacific. *Journal of Climate*, *23*(3), 634–648. https://doi.org/10.1175/2009jcli2904.1

Platnick, S., King, M. D., Ackerman, S. A., Menzel, W. P., Baum, B. A., Riedi, J. C., & Frey, R. A. (2003). The MODIS cloud products: Algorithms and examples from Terra. *IEEE Transactions on Geoscience and Remote Sensing*, *41*(2), 459–473. https://doi.org/10.1109/tgrs.2002.808301

Qu, X., Hall, A., Klein, S. A., & Caldwell, P. M. (2014). On the spread of changes in marine low cloud cover in climate model simulations of the 21st century. *Climate Dynamics*, *42*(9-10), 2603–2626. https://doi.org/10.1007/s00382-013-1945-z

Qu, X., Hall, A., Klein, S. A., & DeAngelis, A. M. (2015). Positive tropical marine low-cloud cover feedback inferred from cloud-controlling factors. *Geophysical Research Letters*, *42*, 7767–7775. https://doi.org/10.1002/2015GL065627

Rayleigh, L. (1916). LIX. On convection currents in a horizontal layer of fluid, when the higher temperature is on the under side. *Philosophical Magazine Series 6*, *32*(192), 529–546. https://doi.org/10.1080/14786441608635602

Reynolds, R. W., Rayner, N. A., Smith, T. M., Stokes, D. C., & Wang, W. (2002). An improved in situ and satellite SST analysis for climate. *Journal of Climate*, *15*(13), 1609–1625. https://doi.org/10.1175/1520-0442(2002)015%3C1609:aiisas%3E2.0.co;2

Rosenfeld, D., Kaufman, Y. J., & Koren, I. (2006). Switching cloud cover and dynamical regimes from open to closed Benard cells in response to the suppression of precipitation by aerosols. *Atmospheric Chemistry and Physics*, *6*(9), 2503–2511. https://doi.org/10.5194/acp-6-2503-2006

Sandu, I., & Stevens, B. (2011). On the factors modulating the stratocumulus to cumulus transitions. *Journal of the Atmospheric Sciences*, *68*(9), 1865–1881. https://doi.org/10.1175/2011jas3614.1

Savic-Jovcic, V., & Stevens, B. (2008). The structure and mesoscale organization of precipitating stratocumulus. *Journal of the Atmospheric Sciences*, *65*(5), 1587–1605. https://doi.org/10.1175/2007jas2456.1

Schultz, D. M. (2001). Reexamining the cold conveyor belt. *Monthly Weather Review*, *129*(9), 2205–2225. https://doi.org/10.1175/1520-0493(2001)129%3C2205:rtccb%3E2.0.co;2

Seethala, C., Norris, J. R., & Myers, T. A. (2015). How has subtropical stratocumulus and associated meteorology changed since the 1980s? *Journal of Climate*, *28*(21), 8396–8410. https://doi.org/10.1175/JCLI-D-15-0120.1

Shao, Q. Q., & Randall, D. A. (1996). Closed mesoscale cellular convection driven by cloud-top radiative cooling. *Journal of the Atmospheric Sciences*, *53*(15), 2144–2165. https://doi.org/10.1175/1520-0469(1996)053%3C2144:cmccdb%3E2.0.co;2

Stevens, B., Vali, G., Comstock, K., Wood, R., van Zanten, M. C., Austin, P. H., … Lenschow, D. H. (2005). Pockets of open cells and drizzle in marine stratocumulus. *Bulletin of the American Meteorological Society*, *86*(1), 51–57. https://doi.org/10.1175/bams-86-1-51

Tomassini, L., Field, P. R., Honnert, R., Malardel, S., McTaggart-Cowan, R., Saitou, K., … Seifert, A. (2016). The "Grey Zone" cold air outbreak global model intercomparison: A cross evaluation using large-eddy simulations. *Journal of Advances in Modeling Earth Systems*, *9*(1), 39–64. https://doi.org/10.1002/2016MS000822

Trenberth, K. E., & Fasullo, J. T. (2010). Simulation of present-day and twenty-first-century energy budgets of the Southern Oceans. *Journal of Climate*, *23*(2), 440–454. https://doi.org/10.1175/2009jcli3152.1

Vogel, R., Nuijens, L., & Stevens, B. (2016). The role of precipitation and spatial organization in the response of trade-wind clouds to warming. *Journal of Advances in Modeling Earth Systems*, *8*(2), 843–862. https://doi.org/10.1002/2015MS000568

Webb, M., Senior, C., Bony, S., & Morcrette, J.-J. (2001). Combining ERBE and ISCCP data to assess clouds in the Hadley Centre, ECMWF and LMD atmospheric climate models. *Climate Dynamics*, *17*(12), 905–922. https://doi.org/10.1007/s003820100157

Wielicki, B. A., Barkstrom, B. R., Harrison, E. F. III, Lee, R. B., Smith, G. L., & Cooper, J. E. (1996). Clouds and the Earth's Radiant Energy System (CERES): An Earth observing system experiment. *Bulletin of the American Meteorological Society*, *77*(5), 853–868. https://doi.org/10.1175/1520-0477(1996)077%3C0853:catere%3E2.0.co;2

Williams, K. D., Bodas-Salcedo, A., Déqué, M., Fermepin, S., Medeiros, B., Watanabe, M., … Williamson, D. L. (2013). The transpose-AMIP II experiment and its application to the understanding of Southern Ocean cloud biases in climate models. *Journal of Climate*, *26*(10), 3258–3274. https://doi.org/10.1175/jcli-d-12-00429.1

Wood, R. (2006). Relationships between optical depth, liquid water path, droplet concentration, and effective radius in an adiabatic layer cloud.

Wood, R. (2012). Stratocumulus clouds. *Monthly Weather Review*, *140*(8), 2373–2423. https://doi.org/10.1175/mwr-d-11-00121.1

Wood, R., & Bretherton, C. S. (2006). On the relationship between stratiform low cloud cover and lower-tropospheric stability. *Journal of Climate*, *19*(24), 6425–6432. https://doi.org/10.1175/JCLI3988.1

Wood, R., Bretherton, C. S., Leon, D., Clarke, A. D., Zuidema, P., Allen, G., & Coe, H. (2011). An aircraft case study of the spatial transition from closed to open mesoscale cellular convection over the Southeast Pacific. *Atmospheric Chemistry and Physics*, *11*(5), 2341–2370. https://doi.org/10.5194/acp-11-2341-2011

Wood, R., & Hartmann, D. L. (2006). Spatial variability of liquid water path in marine low cloud: The importance of mesoscale cellular convection. *Journal of Climate*, *19*(9), 1748–1764. https://doi.org/10.1175/jcli3702.1

Wyant, M. C., Bretherton, C. S., Rand, H. A., & Stevens, D. E. (1997). Numerical simulations and a conceptual model of the stratocumulus to trade cumulus transition. *Journal of the Atmospheric Sciences*, *54*(1), 168–192. https://doi.org/10.1175/1520-0469(1997)054%3C0168:nsaacm%3E2.0.co;2

Xue, H. W., Feingold, G., & Stevens, B. (2008). Aerosol effects on clouds, precipitation, and the organization of shallow cumulus convection. *Journal of the Atmospheric Sciences*, *65*(2), 392–406. https://doi.org/10.1175/2007jas2428.1

Yamaguchi, T., & Feingold, G. (2015). On the relationship between open cellular convective cloud patterns and the spatial distribution of precipitation. *Atmospheric Chemistry and Physics*, *15*(3), 1237–1251. https://doi.org/10.5194/acp-15-1237-2015